



# MONASH University

**The effect of silver current collector on the performance of palm shell  
powered Direct Carbon Fuel Cell**

Khor Hong Weng  
BEng (Hons)

A thesis submitted for the degree of Master at  
Monash University in 2017  
Faculty of Engineering, School of Engineering

## **Copyright notice**


### **Notice 1**

© Khor Hong Weng (2017).

Under the Copyright Act 1968, this thesis must be used only under the normal conditions of scholarly fair dealing. In particular no results or conclusions should be extracted from it, nor should it be copied or closely paraphrased in whole or in part without the written consent of the author. Proper written acknowledgement should be made for any assistance obtained from this thesis.

## Declaration

This thesis contains no material which has been accepted for the award of any other degree or diploma at any university or equivalent institution and that, to the best of my knowledge and belief, this thesis contains no material previously published or written by another person, except where due reference is made in the text of the thesis.

Signature: ...  ....

Print Name: Khor Hong Weng

Date: 25th November 2017

# Table of Contents

<b>Abstract.....</b>	<b>6</b>
<b>List of Figures.....</b>	<b>8</b>
<b>List of Tables .....</b>	<b>9</b>
<b>Acknowledgements .....</b>	<b>10</b>
<b>Chapter 1. Introduction.....</b>	<b>11</b>
1.1 Background.....	11
1.2 Research Motivations.....	17
1.3 Research Objectives.....	19
 <b>Chapter 2. Literature review .....</b>	 <b>21</b>
2.1 Introduction to DCFC .....	21
2.2 Electrochemical reactions of DCFC .....	21
2.3 Components of DCFC.....	23
2.3.1 Anode.....	23
2.3.2 Cathode .....	23
2.3.3 Electrolyte .....	24
2.3.4 Current collectors.....	24
2.4 Concluding comments .....	35
 <b>Chapter 3. Materials &amp; Experimental methods.....</b>	 <b>36</b>
3.1 Preparation of biomass.....	36
3.2 Pyrolysis treatment of biomass .....	36
3.3 Design and fabrication of DCFC .....	38
3.3.1 Button cell.....	38
3.3.2 DCFC reactor .....	40
3.3.3 Current collector .....	41

3.4 Operation of DCFC.....	44
3.5 Performance evaluation of DCFC.....	46
<b>Chapter 4. Performance analysis of DCFC with platinum and silver current collector leads ....</b>	<b>47</b>
4.1 Overview.....	47
4.2 Results and Discussions.....	47
4.3 Conclusions.....	59
<b>Chapter 5. Performance analysis of DCFC with varied number of current collector leads .....</b>	<b>61</b>
5.1 Overview.....	61
5.2 Results and Discussions.....	61
5.3 Conclusions.....	68
<b>Chapter 6. Performance analysis of DCFC with different configurations of current collector...</b>	<b>69</b>
6.1 Overview.....	69
6.2 Results and Discussions.....	69
6.3 Conclusions.....	77
<b>Chapter 7. Conclusion and Future works.....</b>	<b>78</b>
7.1 Conclusion .....	78
7.2 Future works .....	80
<b>Chapter 8. References.....</b>	<b>82</b>

## Abstract

Direct Carbon Fuel Cells (DCFC) are known to provide efficient energy conversion from coal or biomass derived carbon through electrochemical process at high temperature. It comprises of two electrodes that are separated by a layer of electrolyte, with current collector connecting to electrodes to complete the external circuit. While the majority of the components have been thoroughly researched, current collector is often neglected by researchers. Material with high melting point such as Platinum (Pt) was used as current collector in DCFC to withstand the high-temperature operations, effectively increasing the operation cost of DCFC. Fortunately, advancement of materials utilized in the fuel cell components in recent years has managed to reduce DCFC's operating temperature to an acceptable range and opportunity to reduce the operation cost has surfaced. This investigation aims to study the impact on DCFC performance when silver (Ag) is used as current collectors at anode and cathode and at the same time, evaluating the efficiency of electrons collection of different current collectors configuration. An electrolyte supported button cell fed with 30 mg of pyrolyzed palm shell was connected to a potentiostat instrument through Ag current collectors in two electrodes mode. The DCFC system was heated up to 750 °C and the measurements were analyzed with Linear Sweep Voltammetry (LSV) and Electrochemical Impedance Spectroscopy (EIS) methods. Meanwhile, Pt current collectors were used as a control experiment. The experimental results reveal that the material of current collector used at cathode has an impact on the performance characteristics of DCFC similar to the material of current collector used at anode. Setup with Ag current collectors at anode and cathode has peak power density of 7.3 mW/cm<sup>2</sup> which is 50 % more than setup with Pt current collectors at anode and cathode which has peak power density of 4.2 mW/cm<sup>2</sup>. The usage of Ag current collector lead at the cathode has caused the rate of electrons entering cathode unrestricted which has accelerated

the rate of oxygen ions produced through oxygen reduction reaction. With the established link, knowing that Ag current collector at cathode was the limiting factor in DCFC performance, several methods were examined to uplift the limiting factor caused by cathode process. One of the current collection method studied was by varying number of Ag current collector lead connected to electrodes surfaces using the same method of characterization techniques mentioned previously. Setup with two Ag wires attached to each electrode was found to have peak power density of 10.7 mW/cm<sup>2</sup>, which has 46 % more power density than setup with single Ag wire attached to each electrode at peak power density of 7.3 mW/cm<sup>2</sup>. Another investigation of current collection method was carried out by applying Ag paste in various forms on both electrodes surfaces. A difference of 211% of peak power density was observed where Ag paste in mesh-like form was found to produce 13.4 mW/cm<sup>2</sup> of peak power density while Ag paste in layer form has 4.3 mW/cm<sup>2</sup> of peak power density. In general, the results obtained have proven that the material and configuration of current collector used in DCFC should not be ignored like its counterpart in Solid Oxide Fuel Cell (SOFC). Attentive considerations should be given to the current collector when strategizing the reduction of operation cost of DCFC without compromising its performance.

## List of Figures

Figure 1.1: Total end-point impact for all coal-fuelled cases investigated by Nease, J. and T.A. Adams [15].....	13
Figure 2.1: Principle and schematic of DCFC .....	21
Figure 2.2: Severity of faceting on the surface of Ag mesh after 1048 h at a) 690 °C under air atmosphere; b) 790 °C under air atmosphere; c) 800 °C under Ar atmosphere [34].....	26
Figure 2.3: Point type current collector used by Konsolakis et al. [18] .....	31
Figure 2.4: Layer paste used by Guo, Youmin et al. [35] .....	32
Figure 2.5: Wire mesh used by Canavar, Murat et al. [81] .....	33
Figure 2.6: Mesh-like paste used by Li, Chen et al. [24] .....	34
Figure 3.1: Schematic of setup of pyrolysis.....	37
Figure 3.2: Sieved palm shells ready for pyrolysis process .....	38
Figure 3.3: Pyrolyzed palm shells.....	38
Figure 3.4: Close up look of Anode made of NiO .....	39
Figure 3.5 Close up look of Cathode made of LSM .....	39
Figure 3.6: Cross section view of the DCFC reactor .....	40
Figure 3.7: Cured Ag paste at Cathode .....	41
Figure 3.8: Cured Ag paste at Anode.....	42
Figure 3.9: Schematic of DCFC system.....	45
Figure 4.1: Performance curves of cells prior CP .....	48
Figure 4.2: Performance curves of cells after CP .....	48
Figure 4.3: Nyquist plots of cells before CP. The inset shows the close-up look of the Nyquist plots. ....	50
Figure 4.4: Nyquist plots of cells after CP. The inset shows the close-up look of the Nyquist plots. ....	51
Figure 4.5: Equivalent circuit used for fitting Nyquist plot.....	51
Figure 4.6: Potential as a function of time at 750°C .....	53
Figure 4.7: XRD results of fresh button cell and reacted button cell.....	54
Figure 5.1: V-I curves of cells with 1Ag 1Ag, 1Ag 2Ag, 2Ag 1Ag, and 2Ag 2Ag current collector leads at 750°C .....	62
Figure 5.2: Nyquist plot of cells with 1Ag 1Ag, 2Ag 1Ag, 1Ag 2Ag and 2Ag 2Ag current collectors at 750°C. The inset shows the close-up look of the Nyquist plots.....	63
Figure 5.3: Schematic shows the flows of electrons and oxygen ions in 2Ag 2Ag .....	65
Figure 5.4: Schematic depicting the flow of electrons and oxygen ions in 1Ag 2Ag .....	66
Figure 5.5: Schematic depicting the flow of oxygen ions and electrons in 2Ag 1Ag .....	67
Figure 6.1: V-I curves of Point, Mesh and Layer current collector at 750 °C .....	70
Figure 6.2: Nyquist plots of Point, Mesh and Layer current collector at 750°C. The inset shows the close-up look of the Nyquist plots.....	71
Figure 6.3: Mesh-like paste current collector applied on anode and cathode .....	72
Figure 6.4: Schematic depicting the flow of electrons and oxygen ions in the mesh-like paste current collector .....	73



Figure 6.5: Layer paste current collector applied on anode and cathode .....	75
Figure 6.6: The maximum power density corresponding to contact area to electrode area ratio .....	76

## List of Tables

Table 1.1 Main configurations of DCFC and its advantages and disadvantages .....	16
Table 2.1: Overview of quantity of wire leads of current collector used by researchers .....	30
Table 2.2: Overview of current collector configurations used by researchers .....	30
Table 3.1: Configurations of the experiment setup to assess the impact of material of current collector to DCFC performance .....	42
Table 3.2: Configuration of experiment setup to evaluate the effect of number of current collector lead to the DCFC performance .....	43
Table 3.3: Configuration of experiment setup to evaluate the effect of number of current collector lead to the DCFC performance .....	44
Table 4.1: Performance of cells corresponding to Ag Ag, Pt Ag, Ag Pt and Pt Pt prior and after CP measurements .....	49
Table 4.2: Values of resistors by fitting equivalent circuit (Figure 4.5) into Nyquist plots (Figure 4.3 and Figure 4.4) .....	52
Table 5.1: Performance of cells corresponding to 1Ag 1Ag, 2Ag 1Ag, 1Ag 2Ag and 2Ag 2Ag .....	63
Table 5.2: Values of resistors by fitting equivalent circuit (Figure 4.5) into Nyquist plot (Figure 5.2) .....	64
Table 6.1: Performance of cells corresponding to Point, Mesh and Layer current collectors .....	70
Table 6.2: Values of resistors by fitting equivalent circuit (Figure 4.5) into Nyquist plots (Figure 6.2) ...	72

## Acknowledgements

First and foremost, I would like to take this opportunity to express my gratitude to my supervisors Dr. Estee Yong Siek Ting and Dr. Edward Ooi Chien Wei for their immense knowledge, guidance, motivation and patience throughout the research duration, and for pointing the direction whenever I am lost in the research. I am also grateful for the help that I have received from them to interpret experimental studies and results.

Secondly, I would like to acknowledge the 1<sup>st</sup> year financial support received from the Ministry of Science, Technology, and Innovation (MOSTI) through eScience fund. The financial support has lessened my financial burden and has enabled me to primarily focused on my research.

Thirdly, my research would not be possible without the help from the Technical officers, Mr. Mohamed Isha bin Mohd Ali for laboratory apparatus usage, and Mr. Syed Mohd Khalid for providing help in customized fuel cell reactor fabrication.

Fourthly, I truly appreciate the support and encouragement given by the Research and Development Manager, Ms. Wan Nurul Rukiah Wan Rasdi during the final stage of my thesis writing.

Lastly, to my parents and girlfriend; thank you for encouraging me to step out of my comfort zone to pursue my master studies, and whenever I am on the brink of collapse, they constantly showering me with encouragements, supports, and endless love. They are also my source of inspiration and energy, without their love, patience, and forgiveness this work would not have been possible.

# **Chapter 1.**

## **Introduction**

### **1.1 Background**

Most of the power generated in Malaysia comes from the combustion of fossil fuel such as natural gases and coal [1]. The inefficient conversion of dwindling fossil fuel resources to electrical energy through thermal power plant is deemed to be wasteful. In view of these, highly-efficient power generation technologies and renewable fuels need to be incorporated to reduce reliance on fossil fuels while reducing pollution and greenhouse gas emission.

Fuel cells are long regarded as an alternative energy technology to the conventional power generation system due to its high efficiency in energy conversion and low emission of pollutants characteristics [2-4]. Ever since its first inception in the year 1839 by Sir William Grove [5], various types of fuel cells such as Proton Exchange Membrane Fuel Cell (PEMFC), Direct Methanol Fuel Cell (DMFC), Alkaline Fuel Cell (AFC), Phosphoric Acid Fuel Cell (PAFC), Molten Carbonate Fuel Cell (MCFC), Solid Oxide Fuel Cell (SOFC) and Direct Carbon Fuel Cell (DCFC) were developed. A fuel cell is an electrochemical device that converts the chemical energy of fuels and oxidants into direct current of electricity without a combustion step. It comprises of two electrodes that are separated by a layer of electrolyte, with interconnects connecting to electrodes to complete the external circuit. A generic fuel cell's working mechanism consists of fuel oxidation on anode that releases electrons. The electrons are collected by interconnects and travel through an external circuit to a load. Then, the electrons return to the cathode for oxygen reduction process. Oxygen ions released from the oxygen reduction process then travel from cathode to anode through electrolyte which functions as an ionic conducting membrane, completing the circuit [6]. In contrast, PEMFC has slightly different mechanism where the protons

released from fuel oxidation reaction travel from anode to cathode through a layer of electrolyte to complete the circuit.

DCFC is the only fuel cell technology that can provide theoretical efficiency for solid carbon conversion close to 100% based on the small entropy change associated with the overall cell reaction as shown in Reaction (1) [7-9]. Consequently, DCFC has higher fuel utilization efficiency than MCFC or SOFC operating on hydrogen or natural gas (45~60%), making it one of the most efficient electrochemical power generation systems [9].



Gibbs free energy of reaction,  $\Delta G = -395.4 \text{ kJ/mol}$

Enthalpy of reaction,  $\Delta H = -394.0 \text{ kJ/mol}$

Carbon which can be obtained from coal, cracking of hydrocarbons or biomass charcoal is safe, cheap, abundant, and readily available. In contrast, hydrogen is unsafe to use due to fire and explosion hazards and with limited production capacity that barely keeps up with world demands [10]. Hence, wide implementation of DCFC would not require radical change to infrastructure to accommodate hydrogen or gas based economy [11]. Besides that, carbon fuel has a higher energy density (20 kWh/L) both on volumetric and mass density basis compared to alternative fuel sources such as hydrogen with energy density of (2.4 kWh/L) and methane with energy density of (4 kWh/L) [9, 10, 12]. Furthermore, by using processed biomass such as crop residues as fuel, carbon neutral power generation can be acquired since carbon dioxide (CO<sub>2</sub>) emitted in the reaction originates largely from atmospheric CO<sub>2</sub> that is absorbed by the crops via photosynthesis process [13].

Additionally, pure CO<sub>2</sub> is produced in DCFC because carbon oxidation occurs electrochemically at the anode without direct mixing with air. The exclusion of direct contact

between carbon fuel and air has reduced the volume of flue gas to be cleaned by a factor of 5 [14]. Hence, captured CO<sub>2</sub> can be easily sequestered, minimizing the impact on human health and environment as shown by detailed cradle-to-grave life cycle analyses conducted by Nease, J. and T.A. Adams between state of the art coal plants and solid oxide fuel cell utilizing coal [15]. The effect of upstream portions of supply chain and environmental factors such as resource depletion, human health impacts and acid rain formation of both systems were considered. Based on Figure 2.1, coal-fuelled SOFC coupled with carbon captured system (SOFC-C-CCS) has low human health endpoint impacts amongst the power generation type [15]. Nonetheless, resource depletion on SOFC-C-CCS still can be observed due to the usage of coal.

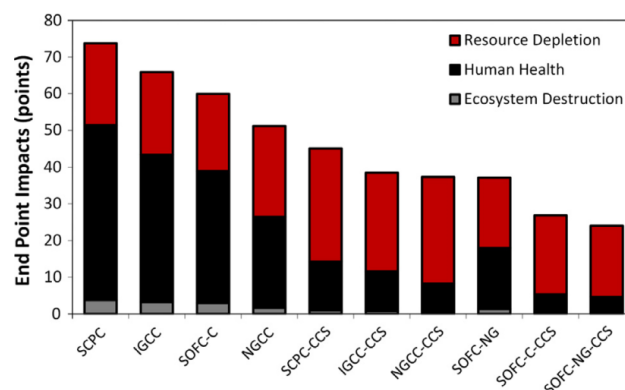


Figure 1.1: Total end-point impact for all coal-fuelled cases investigated by Nease, J. and T.A. Adams [15]

Despite all the advantages, DCFCs do have disadvantages and majority of them stem from the high operating temperature requirement of DCFCs at 650~900 °C to maintain an excellent ionic conductivity of its YSZ electrolyte [2]. The disadvantages of DCFCs are slow start-up and shut-down time, requires significant thermal shielding and high capital investment due to the expensive high temperature materials [2]. In addition, the complex solid feed system for delivery of fuel to the reaction sites of DCFCs has placed DCFCs in disadvantage against liquid fuel fed fuel cell systems [2].

The flexibility of DCFC to adapt wide variety of fuels to generate electric energy electrochemically yet offers high system efficiency compared to other fuel cell system has attracted significant interest of researchers in the development of DCFC [4]. One of the interesting findings was the successful application of carbonaceous biomass such as almond shell, [13] pine charcoal [16], olive wood [17], pistachio shell [18] and coconut charcoal [19] in DCFC. Most of the experimental results of research groups [13, 16-19] have indicated that carbonaceous biomasses need to possess high fixed carbon content and fewer crystalline structures to yield DCFC performance that was comparable to coal. Besides that, high oxygen functional group in carbonaceous biomasses was also pointed out to have enhanced the DCFC performance [13, 16]. The successful application of carbonaceous biomasses has demonstrated that there is a possibility to use palm shell as fuel for DCFC in Malaysia since Malaysia is the second largest palm oil export country in the world.

There are three main configurations of DCFC under development which are typically differentiated by the type of electrolyte used as shown in Figure 2.3. They are molten hydroxide (MH-DCFC), molten carbonate (MC-DCFC) and solid oxygen ion conducting ceramic (SO-DCFC) [2, 9, 14, 20]. Firstly, MH-DCFC uses molten hydroxides such as molten sodium hydroxide and potassium hydroxide as its electrolyte. The hydroxide ions possess high ionic conductivity, enabling MH-DCFC to operate at relative low temperature of 450 °C. Nevertheless, the formation of carbonate in the electrolyte has halted the operations of MH-DCFC. Efforts to minimize the formation of the carbonate however, has complicated the design and reaction mechanism of the MH-DCFC [10, 21].

Secondly, MC-DCFC operates at a similar concept to MH-DCFC except that the molten carbonate is used as electrolyte and it operates at a higher temperature of 600 – 850 °C. The

utilization of molten carbonate has resulted in a more stable operation in the presence of CO<sub>2</sub> and has extended the contact area between the carbon and the electrolyte [20]. Nonetheless, the vaporization of the electrolyte and corrosion of cell components has led to instability of the system in long run [22].

Lastly, SO-DCFC comprises a solid oxygen-ion conducting electrolyte. The solid state electrolyte which acts as a structural support for the cell ensures optimum distribution of electrolyte [23] and minimum cell degradation due to the absence of highly corrosive liquids as in the two configurations mentioned above [20]. Two most common designs for SO-DCFC are tubular and planar [2]. Tubular SO-DCFC, as its name implies, comprises of electrolyte layer in tube formation. The tube form electrolyte provides excellent sealing to prevent mixing of fuel and air that will degrade the cell performance. However, the complexity of manufacturing processes of the complex geometry of tubular design has led to a system with lower overall power density and higher manufacturing cost [2]. Meanwhile, planar SO-DCFC comprises a flat electrolyte layer which facilitates simpler manufacturing processes, thus reducing the manufacturing cost and exhibits good repeatability [24]. Table 1.1 summarizes the main configurations of DCFC and its associated advantages and disadvantages.

Table 1.1 Main configurations of DCFC and its advantages and disadvantages

Type of DCFC (Differentiated by conducting ions)	Reactions	Sub- categories	Advantages	Disadvantages
Molten Hydroxides (OH <sup>-</sup> )	Anode: $C + 4OH^- \rightarrow CO_2 + 2H_2O + 4e^-$ Cathode: $O_2 + 2H_2O + 4e^- \rightarrow 4OH^-$	-	Higher ionic conductivity Low temperature of 450 °C	Formation of carbonate in the electrolyte has halted the operations
Molten Carbonates (CO <sub>3</sub> <sup>2-</sup> )	Anode: $C + 2CO_3^{2-} \rightarrow 3CO_2 + 4e^-$ Cathode: $O_2 + 2CO_2 + 4e^- \rightarrow 2CO_3^{2-}$	-	Extended the contact area between the carbon and the electrolyte	Vaporization of the electrolyte and corrosion of cell components
Oxygen ion conducting ceramic (O <sup>2-</sup> )	Anode: $C + 2O^{2-} \rightarrow CO_2 + 4e^-$ Cathode: $O_2 + 4e^- \rightarrow 2O^{2-}$	Tubular	Excellent sealing to prevent mixing of fuel and air	Lower overall power density and higher manufacturing cost
		Planar	Low manufacturing cost and exhibits good repeatability	Prone to sealing leakage

Despite the different shapes of DCFC, current collectors in various sort of forms and materials are used to collect electrons generated from fuel oxidation at anode and distribute the electrons to cathode for oxygen reduction process.



## 1.2 Research Motivations

DCFC in laboratory scale are often simplified to fuel cell and current collection meshes and wires. Platinum (Pt) was a popular material choice for the current collector due to the high melting point it possessed to withstand the high operating temperature of DCFC [24-33]. However, due to its rarity in the earth crust, the usage of Pt as current collector was one of the factors that contribute to the high capital investment of DCFC. Silver (Ag), which has a low electronic resistivity of  $1.63 \times 10^{-8} \Omega\text{m}$ , melting point of  $961.78^\circ\text{C}$  yet cheaper than Pt seems to be a good candidate for Pt replacement in DCFC. Despite fulfilling the criteria, Ag was found to have weight reduction due to vaporization at  $790^\circ\text{C}$  with the vaporization rate of  $1.29 \mu\text{gcm}^{-2} \text{h}^{-1}$  [34]. The reduction of operating temperature to  $690^\circ\text{C}$  was found to significantly reduced the vaporization rate of Ag to  $0.094 \mu\text{gcm}^{-2} \text{h}^{-1}$ , indicating that vaporization of Ag was greatly dependent on the operating temperature of DCFC [34]. Nevertheless, the reduction in operating temperature has caused an increase in resistance in electrodes, affecting the overall DCFC performance. Hence, a search for a balance point between the stability of Ag and the performance of DCFC is warranted.

There are several configurations of current collector applied on surface of electrode adopted by researchers in laboratory scale. They are single contact point [18, 35], layer paste [17, 36], mesh-like paste [24, 37, 38] and wire mesh [25, 26, 39, 40] configuration. Foam was observed to be used in isolated case [41]. There are no studies on current collector configurations conducted in DCFC environment which can be referred to. Fortunately, the studies to understand the effect of current collector configurations to the performance of SOFC can be used as reference due to the similarity of the fuel cell mechanism between DCFC and SOFC albeit in different fuel environment. One of the studies by Chen Yubo et al. revolved around paste layer and mesh-like paste [37] in SOFC. The Area Specific Resistance (ASR) of paste layer increase over the time

from 0.10 to 0.16  $\Omega \text{ cm}^2$  while the ASR of mesh-like paste remained stable at 0.15  $\Omega \text{ cm}^2$ . Another study by Guo Youmin et al. revolved around point contact and layer paste [35] in SOFC. The point contact configuration has exhibited ASR of 23.9  $\Omega \text{ cm}^2$  which is significantly higher than the layer paste configuration which has 1.9  $\Omega \text{ cm}^2$ . Meanwhile, the quantity of current collector leads used in each experiment was observed to differ from research groups. Some are using one current collector lead per electrode [8, 35, 42-44], while some are using two current collector leads per electrode [24, 33, 45]. Increasing contact area between the current collector and the electrodes was found to decrease the overall cell resistance [46]. Hence, the impact of the quantity of current collector leads to the performance of fuel cells mentioned above is unknown for the moment. Besides that, Guo Youmin et al. has found that different current collection strategies employed by the researchers have caused large discrepancies in the power outputs of cells despite the cells configuration and fabrication processes are similar while compiling the performance of various electrodes published by the researchers [35]. For example, a discrepancy of 20 % for the peak power density values was observed despite two similar cells were tested at the same temperature but with different current collector configurations. The conclusion has emphasized that it was crucial to adopt proper current collection method to assess the performance of the electrodes accurately.

### 1.3 Research Objectives

Silver (Ag), which has the potential to replace platinum (Pt) in DCFC suffers from vaporization at 800 °C as mentioned in Section 1.2. However, the vaporization rate of Ag can be reduced with lower operating temperature. Hence, the first objective of the research is to examine the feasibility of Ag to replace Pt as current collectors at 750 °C.

The contact resistance between the electrode and current collector plays a major role in the total cell resistance in DCFC. Hence, the choice of a suitable current collector is important to understand the electrochemical behavior of DCFC. Nevertheless, the current collector reported in literature often varies and is sometimes not mentioned. The second objective of the research is to search for the best current collection configuration for DCFC by manipulating the quantity of current collector lead attached to the electrodes and the shape of the current collector applied to the electrode surface.

The specific aims of this research are as below:

- i. To investigate the electrochemical performance of DCFC at 750 °C when Ag current collectors are attached to the electrodes. The investigation was done by varying the material used at the anode and cathode current collectors leads in between Pt and Ag, followed by quantifying the electrochemical performance and the stability of DCFC. If Ag current collector has higher peak power density and lower ASR than Pt current collector, then Ag current collector can be considered as an alternative to Pt current collector.
- ii. To understand the implications of using different quantity of current collection leads on the electrochemical performance of DCFC at 750 °C. The study was conducted by manipulating the current collector lead quantity attached to the electrode surfaces, followed by measuring

the electrochemical performance of DCFC. Setup with highest peak power density and lowest ASR has better electron collection efficiency.

- iii. To understand the implications of using different current collection configuration on the electrochemical performance of DCFC at 750 °C. The study was conducted by varying the Ag paste configuration applied on the electrode surfaces, followed by measuring the electrochemical performance of DCFC. Setup with highest peak power density and lowest ASR has better electron collection efficiency.

## Chapter 2.

### Literature review

#### 2.1 Introduction to DCFC

Fuel cells have long been foreshadowed as a replacement for current power generation technologies that are inefficient. DCFC which is the only fuel cell technology that utilizes solid carbon fuel for electricity generation is starting to gain tractions in recent years because of the resilient synergistic advantages it possessed as discussed in Chapter 1.

#### 2.2 Electrochemical reactions of DCFC

The overall DCFC reaction (1) is derived from the mechanism happened in anode and cathode as shown in Figure 2.1.

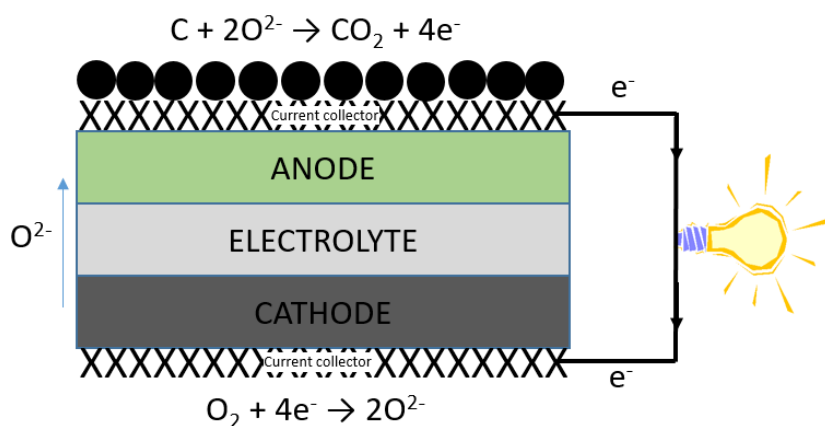


Figure 2.1: Principle and schematic of DCFC

Oxygen ( $O_2$ ) supplied to cathode will be reduced to oxygen ion ( $O^{2-}$ ) by reacting with electrons ( $e^-$ ) accumulated on the cathode.



Next, the  $O^{2-}$  will migrate across electrolyte from cathode to anode, and it will react with solid carbon (C) at anode to produce  $CO_2$ . Electrons are released during the process of carbon oxidation.



The produced electrons travel from anode to cathode through current collector that act as an external circuit. The flow of electrons from anode to cathode produces electric current.

In reality, a mixture of direct and indirect carbon oxidation reactions occurs inside anode chamber instead of simple electrochemical Reaction (3).  $CO_2$  can be produced by having carbon particles that have direct contact with the anode to react with oxygen ions via the following reaction sequence:



Carbon particles that do not have direct contact with anode will be oxidized by the following reaction sequence:



Reaction (6) requires the presence of  $CO_2$  produced via reaction (3) and (5) if  $CO_2$  is not used as the anode purge gas. The formation of carbon monoxide (CO) via Boudouard reaction within anode will likely occur spontaneously at temperature above 700 °C [2].

## **2.3 Components of DCFC**

Many of the design features such as materials used for cell components are rather in common despite several sub-classes of SO-DCFC as already outlined above. This section covers a few well-established design characteristics of the modern SO- DCFC. The SO-DCFC typically comprises of four general components which are anode, cathode, electrolyte and current collector.

### **2.3.1 Anode**

The basic requirement for the selection of material of anode is that it must be conductive of ions and electrons. To fulfill this demand, the anode is made from a cermet, which is a mixture of ceramic, “cer” and a metal, “met” [11]. Traditionally, the cermet used in anode consists of metal Nickel (Ni) and ceramic Ytria Stabilized Zirconia (YSZ) for its high catalytic activity and porous structure to ease gas diffusion. Nevertheless, pure nickel metal is rarely used as anode due to the large difference in expansion coefficient between nickel and ceramic electrolyte which causes flaking issue on anode [47].

### **2.3.2 Cathode**

Likewise, the material of cathode must be conductive of electrons and ions. The cathode is typically composed of Lanthanum Strontium Manganite (LSM) due to its relatively high thermal and chemical stability at high temperature and highly oxidizing environment and has excellent compatibility with YSZ in thermal expansion. As the operating temperature of DCFC is reduced below 950 °C, LSM is often mixed with YSZ powder to minimize the resistance of the LSM cathode to about 0.1  $\Omega$  for 1 cm<sup>2</sup> [47].

### **2.3.3 Electrolyte**

The desirable properties of an electrolyte are low electronic conductivity to minimize current leakage from the anode, and high ionic conductivity. The electrolyte material is made from oxygen-ion-conducting solid ceramic Yttria stabilized zirconia (YSZ), Scandia stabilized zirconia (ScSZ) or Gadolinium Stabilized Ceria (GDC) [2]. The usage of ceramic based electrolyte means that the corrosion of vital cell components is minimal at high temperature which is required to maintain the high ionic conductivity of YSZ. Nonetheless, there are several research efforts focused on reducing the high temperature requirement of electrolyte to allow for lower temperature cell operation. One of the methods is to reduce the thickness of the electrolyte to shorten the travel distance of  $O^{2-}$  ions which eventually reduces the ion transport resistance [48]. However, sufficient electrolyte thickness is still crucial to prevent short-circuited cell caused by current leakage [11].

### **2.3.4 Current collectors**

#### **2.3.4.1 Material of current collector**

Current collectors gather electrons produced at the anode and allow them to flow to the cathode through external circuit because YSZ electrolyte is a non-electronic conductive material and it only allows oxygen ions to flow through it. Platinum (Pt) is the most popular choice among researchers to incorporate it in high-temperature DCFC [24-33] because it is the least reactive metal and has excellent corrosion resistance, which are excellent properties for prolonging current collector usage in DCFC. Other than that, Pt has a high melting point (1768 °C) that can withstand the high operating temperature of 800 – 950 °C required for DCFC electrolyte made of YSZ to maintain its high ionic conductivity. Nonetheless, the rarity of Pt in earth crust plus high demand



of Pt usages have led the price of Pt increased to an average of USD 1,100 per oz. [49] which makes it less desirable for use in DCFC applications [50-52].

Meanwhile, silver (Ag) which has a melting point of 961 °C, lowest electronic conductivity (15.87 nΩ.m) yet cheaper than Pt which is at USD 15 per oz. [53] has become an attractive material to replace Pt after reduction of operating temperature down to 800 °C due to the advancement of material in the button cell. Experiments that used Ag as current collectors were available in the literature [37, 45, 54-58]. However, most of them were in SOFC with a few exceptions in SO-DCFC. There were reported instability of Ag at high temperature. For example, during the 1960s, Ag was used as cathode material and current collector of DCFC system but later was replaced by other cathode materials due to it possessed high volatility and large thermal expansion coefficient at 1000 °C which was the operation temperature of DCFC at that time [54]. Besides that, the evaporation rate of Ag was greatly depended on the surrounding atmosphere, specimen geometry, specimen surface, and gas velocity as shown by the experiment conducted by Meulenberg et al. [34]. Ag exposed to air at 790 °C has exhibited approximately 14 times higher of mass loss than Ag exposed to air at 690 °C and Ag exposed to Argon (Ar) at 800 °C after 40,000 hours of testing [34]. Other than that, thermal faceting was observed on the surface of metals when metals were heated at a temperature just below the melting point of the metals in the presence of oxygen [59]. Nevertheless, more attention was given to Ag as shown by several researchers [34, 59, 60]. For example, pronounced faceting was observed on the surface of Ag exposed to air at 790 °C while Ag exposed to Ar at 800 °C did not have structural changes as shown in Figure 2.2 [34].

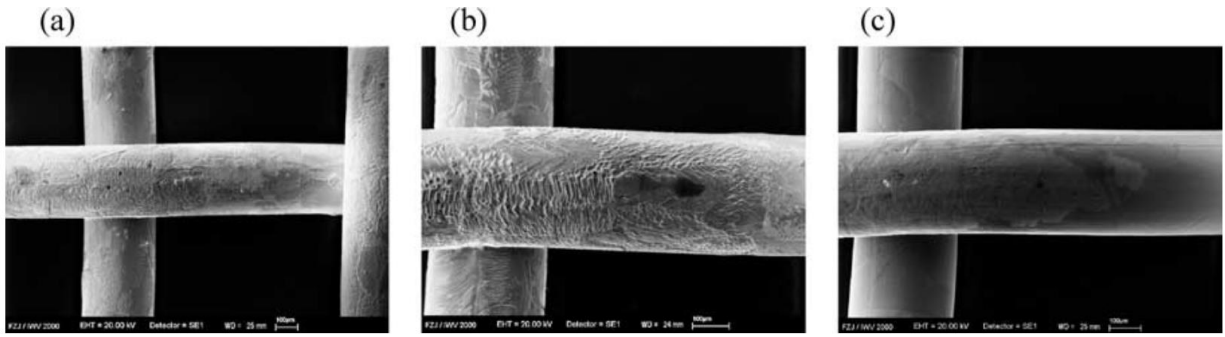


Figure 2.2: Severity of faceting on the surface of Ag mesh after 1048 h at a) 690 °C under air atmosphere; b) 790 °C under air atmosphere; c) 800 °C under Ar atmosphere [34]

Moreover, migration of Ag into SOFC was observed and the migration has been induced by two mechanisms as described by two group of researchers. Janek and Korte have suggested that diffusion of Ag induced by temperature and concentration gradients was called thermo-migration [61] while Ho PS and Huntington HB found out that diffusion driven by electrical forces was known as electro-migration [62]. Thermo-migration is a phenomenon where transport of mass was induced by temperature and concentration gradient. Meanwhile, electro-migration is a phenomenon where transport of mass was induced by transfer of momentum from electron to atom. The migration of Ag atoms has reduced the contact area between current collector and electrodes, effectively limiting the triple phase boundary of DCFC. To put the two mechanisms to test, De Silva et al. have devised an experiment to observe Ag migration in SOFC fuelled by syngas. Two sets of cell were tested where one operated in open circuit mode while another set operated in closed circuit mode. Ag migration occurred in the cell tested in closed circuit mode at 900 °C for 200 hours potentiostatically at 0.7 V [45]. A similar outcome was observed in Simner, S.P. et al. experiment where migration from Ag current collectors was found in the interface of cathode and electrolyte while performing 0.7 V potentiostatic test for 450 hours at 750 °C but not in 50 hours of open circuit test [63]. Although both research groups have shown that Ag migration was induced

by electro-migration, it was hard to conclude that Ag migration in the SOFC was solely from electro-migration as it was able to generate heat due to current flow and resistive heating [45]. Furthermore, several researchers have conducted experiments to study the interaction between Ag and oxygen at multiple temperature ranges. It was found that oxidation occurs only at a temperature below 260-315 °C and no oxide formation occurs at higher temperature due to decomposition of silver oxide (AgO) to form metallic Ag [64-66].

In the meantime, copper (Cu) has a melting point of 1084 °C and is a well-known ductile transition metal with low electronic resistivity (16.78 nΩ.m) second to Ag. It is widely adopted in electrical wires and cables due to its relatively low market price compared to Ag which is USD 2.38 per oz. Nonetheless, it is rarely used in DCFC as current collector in elevated temperature condition due to the rate of Cu oxidation increases exponentially in an oxygen environment. Two layers of corrosion compounds were formed which were Cu<sub>2</sub>O and CuO respectively as confirmed by researchers [67-70]. Copper oxide electronic resistivity was found to be in the range of 10<sup>7</sup> Ω.m at 800 °C [71] and will impact the efficiency of electrons collection.

Pt and Ag were known to possess excellent oxygen reduction properties [57, 72, 73] and excellent carbon oxidation properties [26, 56]. Hence, the usage of Pt and Ag as current collectors will interfere with the reactions at electrodes, affecting the overall performance of the DCFC. Unfortunately, there were limited studies on the influence of different metals current collector towards the performance of the DCFC which can be referenced. For example, Simner, S.P. et al. have compared the performance of the hydrogen (H<sub>2</sub>) fuelled SOFC that utilized Pt and Ag current collectors at the cathode [63]. SOFC with Pt current collector has higher power density than the one with Ag current collector with the values of 0.5 W/cm<sup>2</sup> and 0.4 W/cm<sup>2</sup>, respectively. Based on the cross section of the reacted planar SOFC cells, both Pt and Ag have migrated into the cathode

layer, but with different deposition characteristics. Besides that, Deleebeeck et al. have studied the electrochemical performance of Hybrid DCFC by varying current collectors at anode at 800 °C [56]. Both Pt and Ag current collectors have shown chemical stability in molten alkali carbonate and offered maximum power density of 23 mW/cm<sup>2</sup> and 19.8 mW/cm<sup>2</sup>, respectively. The marginal advantage in terms of maximum power density provided by Pt suggested that Pt could be a better carbon oxidation catalyst than Ag in molten carbonate. Nonetheless, the comparison of Pt and Ag performed by Deleebeeck et al. and Simner, S.P. et al. were incomplete due to the lack of comparison in terms of resistance. Z. H. Bi and J. H. Zhu have studied the effect of Pt and Ag as current collector at anode of H<sub>2</sub> fuelled SOFC [74]. Likewise, anode with Pt current collector exhibited higher maximum power density at 960 mW/cm<sup>2</sup> than anode with Ag current collector at 150 mW/cm<sup>2</sup>. In terms of total resistance, anode with Pt current collector has halved of the value of anode with Ag current collector at 0.32 Ωcm<sup>2</sup> and 0.68 Ωcm<sup>2</sup>, respectively. Anode with Pt current collector has exhibited better performance than anode with Ag current collector due to the fact the Pt was an excellent catalyst for oxidation of H<sub>2</sub> [74]. Nevertheless, the comparison of the performance might not be accurate as the mesh size used for Pt and Ag current collector was different and this will affect the contact points between current collector and anode.

The examples above show that using different materials for current collectors at anode or cathode will influence the performance of the overall fuel cell. However, there were contradicting findings on which side of the electrodes will have a greater impact on the overall DCFC performance. In SOFC, the interface resistance between anode and current collector was found negligible while cathode and current collector interface contributed the largest part to the electron transmission resistance [75, 76]. Overall cell impedance and polarization losses were significantly reduced with the increase in the contact area in between current collector and cathode [46]. On the

contrary, in DCFC, both low and high-frequency arcs in the impedance spectra were mainly contributed by anode because resistances contributed by cathode at 800 °C were reported to be in the range of 0.1 to 0.2  $\Omega\text{cm}^2$  [7, 77]. A plausible explanation for this phenomenon was that the usage of solid fuels in DCFC has caused slow reaction rate in anode [78].

#### **2.3.4.2 Wire lead of current collector**

Reported literature mostly has a varied number of current collection wire leads attached to the fuel cell and sometimes not mentioned. Ohmic resistance of a fuel cell is attributed to electrical resistance of a materials and contact resistance. Thus, material with high electronic resistance used as wire lead will limit the rate of electrons pass through wire leads from the current collector. Additionally, Jiang, S.P. et al. has concluded that increasing the contact area between the current collector and the electrode will decrease the overall cell resistance [46]. Hence, introducing additional wire lead could decrease contact resistance due to increased contact area between wire leads and current collector that resulted more current to flow through between current collector and wire leads. There are no studies regarding the effect of quantity of current collector wire leads on the overall DCFC performance which can be referenced apart from compiling data from literature. However, the maximum current density compiled from the literature listed in Table 2.1 deviates from the conclusion above made by Jiang, S.P.. The performance deviations were mainly caused by different type of fuels, active area of electrode and configuration of current collector used in the literature which made it tedious for comparison studies.

Table 2.1: Overview of quantity of wire leads of current collector used by researchers

Wire leads	Active area (cm <sup>2</sup> )	Max. current	References
		density (mA/cm <sup>2</sup> )	
2 wires per side	1.54	10	[24]
1 wire per side	16	312	[44]
1 wire per side	0.5	100	[8]

### 2.3.4.3 Configurations of Current collector

Current collector serves as a network for the electrons produced from electrochemical reactions at the anode to move to the cathode for oxygen reduction process. Hence, the configuration of the current collector will affect the DCFC performance, and it is important to understand the working mechanism. The common configurations adopted by researchers in laboratory scale were the single contact point, paste layer, and mesh-like paste and wire mesh. Nevertheless, a direct comparison could not be made due to the different type of fuels, active area of electrode and configuration of fuel cell used in the literature which is shown in Table 2.2.

Table 2.2: Overview of current collector configurations used by researchers.

Current collector configurations	Peak Power density (mW/cm <sup>2</sup> )	Total resistance ( $\Omega$ cm <sup>2</sup> )	References
Point paste	8	2	[18]
Layer paste	150	1	[79]
Layer paste	120	-	[17]
Layer paste	50	20	[36]
Wire mesh	3	-	[26]
Wire mesh	86.8	3.2	[39]
Wire mesh	-	-	[40]
Wire mesh	65	-	[80]
Wire mesh	35	6.8	[8]

Mesh-like paste	-	-	[24]
Mesh-like paste	100	2	[38]

#### 2.3.4.3.1 Point paste

Konsolakis M et al. have affixed the wire leads to the center of the electrode surface by using metal paste [18] as shown in Figure 2.3. As the surface area occupied by the metal paste is tiny compared to the electrode surface area, it can be considered as having no current collector applied. The electrochemical performance of DCFC with point paste current collector at cathode demonstrated by Konsolakis M et al. was expectedly low compared to other current collector configurations with a maximum difference of peak power density as large as a factor of 19 at 750 °C. The low performance was caused by the high contact resistance between the cathode and the current collector.

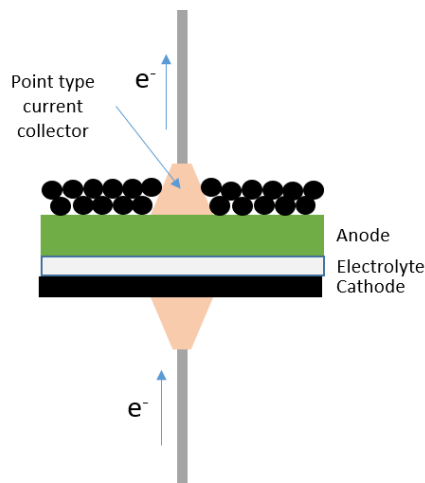


Figure 2.3: Point type current collector used by Konsolakis et al. [18]

#### 2.3.4.3.2 Layer paste

Metal paste covering entire electrode surface was one of the many methods to collect or disperse electrons [17, 36, 79] as shown in Figure 2.4. Diluted metal paste layer was found to have better electrochemical performance when compared to concentrated metal paste layer as proven by Guo, Youmin et al. [35]. The good performance of the diluted Ag paste layer was largely contributed by the huge amount of porosities available in the Ag paste layer for gas diffusion. However, the porous structure of the diluted Ag paste layer collapsed during long-term operation while concentrated Ag paste structure remains unaffected as mentioned by Chen, Yubo et al. [37]. The structural collapse of the diluted Ag paste layer was due to sintering and evaporation of Ag at high-temperature operation.

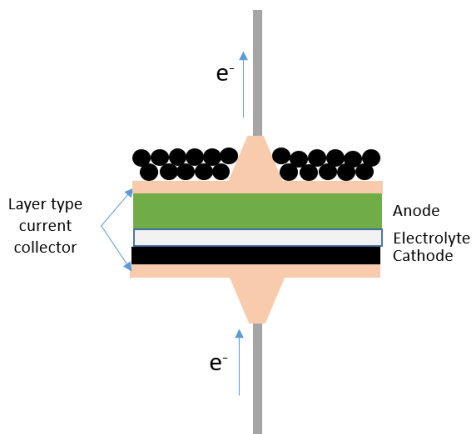


Figure 2.4: Layer paste used by Guo, Youmin et al. [35]

#### 2.3.4.3.3 Wire mesh

Wire mesh is a popular choice among the researchers to use as current collectors [8, 25, 26, 39, 40, 80, 81] as shown in Figure 2.5. This is because of the wire mesh mimics the flow channels of the interconnectors available in the stacked SOFC and provides adequate contact points to the electrodes [81]. The contacts between mesh and electrode surface were made through



crossover points of the mesh. However, not all crossover points were in touch with the electrode because of the warpage of the mesh, causing some of the crossover points not at the same level [46]. This situation has caused difficulty in determining the actual contact points between the mesh and the electrode surface. The spacing between wires in the wire mesh plays a role in the fuel cell performance. K. Sasaki et al. [82] and Jiang, S. P. et al. [46] both agreed that with the increase in contact area between the current collector and cathode surface, cell resistance and overpotential decreased. However, the methods to increase the contact area employed by both researchers were different. K. Sasaki et al. increased the contact area by reducing spacing of Pt meshes current collector embedded in the LSM electrode while Jiang, S.P. et al. increased the contact area of Ag foil contact point. However, there were contradicting conclusions on the spacing of wire mesh in anode from researchers. Canavar, Murat et al. [81] favors spot welded wire mesh with wide wire gap due to having sufficient channel for gas distribution and maintaining good contact between the current collector and the electrode surface. In the meantime, Jiang, S.P. et al. concluded that increasing the contact area of the current collector in anode did not contribute significantly to the overall cell resistance due to the higher ionic conductivity of porous Ni/YSZ cermet on the anode [46].

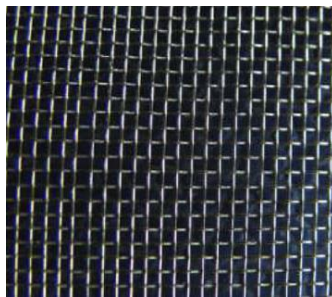


Figure 2.5: Wire mesh used by Canavar, Murat et al. [81]

#### 2.3.4.3.4 Mesh-like paste

There were other researchers applied the paste to electrode surface in a mesh-like morphological structure [24, 37, 38] as shown in Figure 2.6. The intention of implementing the paste in that manner was to mimic wire mesh so that there will be gas diffusion at the electrode surface even when the paste sintered due to long hours of operation at high temperature. Besides that, mesh-like paste provides a larger contact area between electrodes and current collector than the wire mesh, resulting in lower ohmic resistance by a factor of 5 compared to wire mesh [42]. Chen, Yubo et al. [37] have made a comparison of area specific resistance (ASR) between diluted layer paste and mesh-like paste. The results showed that mesh-like paste has higher ASR than diluted layer paste and it was due to a small portion of the electrode surface was covered by Ag paste only. Nevertheless, the mesh-like paste has exhibited a fairly stable structure after subjected to long term stability test, suggesting that the evaporation of Ag from the mesh-like Ag paste in long term operation was insignificant.

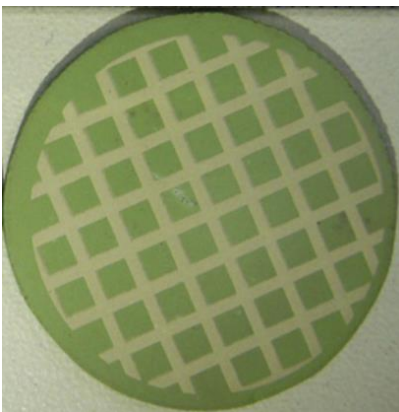


Figure 2.6: Mesh-like paste used by Li, Chen et al. [24]

## 2.4 Concluding comments

Direct carbon fuel cell (DCFC) is the only fuel cell technology that utilizes solid carbon fuel for electricity generation with added advantages such as carbon neutral when biomass carbonaceous fuels are used. The principle electrochemical reactions of DCFC, the different configuration of DCFC, the components of DCFC have been reviewed in this chapter. However, emphasis has been given on review of current collector in particularly its material, wire leads and the configuration of the current collector given that the current collector is one of the cell components that the electrons need to pass through. Inappropriate current collector method employed in the experiments will impact the overall DCFC performance, leading to false conclusions.

Nevertheless, the majority of the research to date has focused on improving the overall cell performance by studying alternative materials for anode and cathode while neglecting current collector. Until recently, only limited number of studies revolved around current collector yet the majority of them are not in DCFC environment. Assessing the effect of current collector on cell performance by comparing the available data in literature is a tedious process as the configuration of experiment setup used by other researchers varied from each other. Aside from that, all of the studies on the current collector in literature are either conducted on anode or cathode. As there are contradicting findings on which side of the electrodes will have a greater impact on the overall DCFC performance, a study on the effect of current collector on both of the electrodes is warranted.

## **Chapter 3.**

### **Materials & Experimental methods**

#### **3.1 Preparation of biomass**

Palm shells used as solid fuel in the experiments were collected from Hulu Langat palm oil mill in Selangor. The palm shells were spread evenly on aluminum foil and air-dried in Memmert oven at 110 °C for 48 hours to remove moisture [83]. Following that, the dried palm shells were pounded into smaller pieces by mortar and pestle. Then, the palm shells were ground using Fritsch Pulverisette 14 Variable Speed Rotor Mill with the blade size of 2 mm and speed of 6000 rpm [83]. The ground palm shells were sieved to obtain 0.25 mm to 0.5 mm particle size, using AS200 CTRL Sieve Shaker. Sieved palm shells were stored in a desiccator for further usage.

#### **3.2 Pyrolysis treatment of biomass**

The schematic of the pyrolysis setup was illustrated in Figure 3.1. Two (2) gram of sieved palm shells were placed on a stainless-steel mesh of a sample holder as shown in Figure 3.2. Subsequently, the filled sample holder was inserted into a stainless-steel tubular reactor, and both open ends of the tubular reactor were covered with gaskets and stainless-steel inlet nozzles. Next, the tubular reactor was placed and secured in the vertical Carbolite VST 12/600 tubular furnace. Then, the top inlet nozzle of the reactor was connected to 99.999 % N<sub>2</sub> gas supply while the bottom inlet nozzle of the reactor was connected to a pipe to direct the output gas to a fume hood. The tubular reactor was supplied with N<sub>2</sub> at 150 mL/min for 15 minutes at room temperature to purge out air molecules that were trapped inside the tubular reactor.

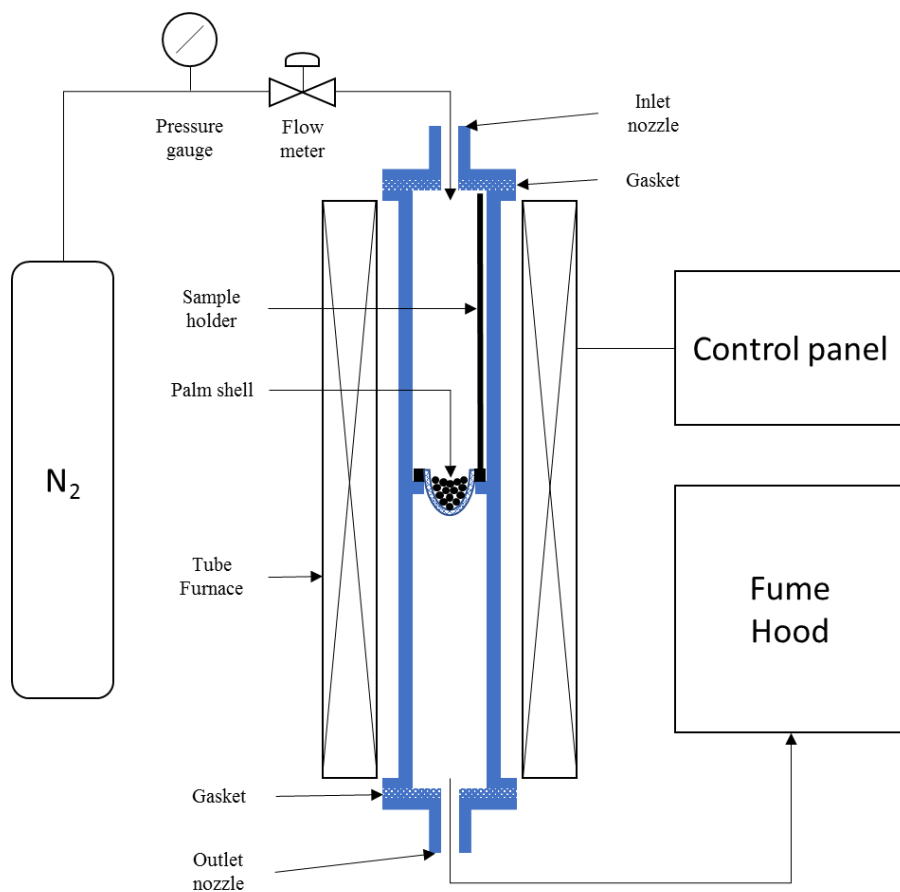


Figure 3.1: Schematic of setup of pyrolysis

The tubular reactor was heated to 600 °C at a heating rate of 10 °C/min for 2 hours, under a continuous flow of  $N_2$  gas. 600 °C was chosen for the pyrolysis temperature because it has been proven to yield maximum performance in DCFC by previous study [83]. The pyrolyzed palm shells as shown in Figure 3.3 were stored at room temperature under dry conditions for future usage.



Figure 3.2: Sieved palm shells ready for pyrolysis process



Figure 3.3: Pyrolyzed palm shells

### **3.3 Design and fabrication of DCFC**

#### **3.3.1 Button cell**

All experiments in this thesis utilized electrolyte-supported fuel cell fabricated by Ningbo SOFCMAN Energy Technology Co., Ltd. as shown in Figure 3.4 and Figure 3.5. The circular planar button cell consists of 10 mm diameter Nickel Oxide (NiO) anode, 20 mm diameter 8 mol % Yttrium Oxide ( $\text{Y}_2\text{O}_3$ ) Fully Stabilized Zirconium Dioxide ( $\text{ZrO}_2$ ) 8YSZ electrolyte, and 10 mm

diameter Lanthanum Strontium Manganite (LSM) cathode with a thickness of  $10 \pm 3 \mu\text{m}$ ,  $200 \pm 3 \mu\text{m}$ , and  $25 \pm 3 \mu\text{m}$ , respectively. The area of anode ( $0.79 \text{ cm}^2$ ) will be used for the calculation of current density, power density and impedance. New button cells were used for each experiment while used button cells were used to check the reproducibility of the experiment's data. The used button cells were heated up to  $800 \text{ }^\circ\text{C}$  in a furnace for 1 hour to ensure the anode was fully re-oxidized.

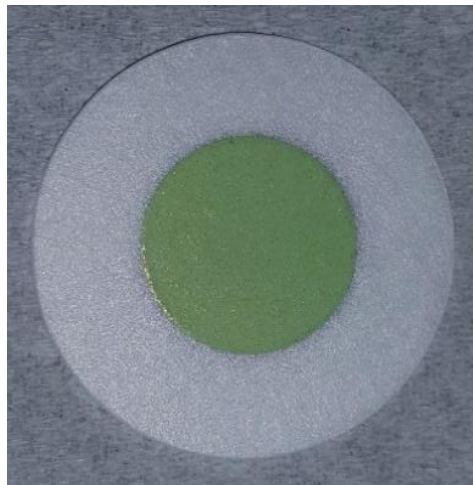


Figure 3.4: Close up look of Anode made of NiO



Figure 3.5 Close up look of Cathode made of LSM

### 3.3.2 DCFC reactor

Figure 3.6 shows the structural design of the DCFC reactor. The DCFC reactor was made up of different sizes of alumina rings and four bores tubes. These parts were glued together by using alumina paste. The four bores tube served as current collector lead tunnels, gas inlet and outlet for both anode and cathode reactors, respectively. An external spring system was attached to the anode reactor to push the four bores tube towards the pyrolyzed palm shells to enhance the number of contact points between pyrolyzed palm shells and anode. Also, the spring minimizes the bulk contact resistance between palm shell particles as proven by the results published by P. Desclaux et al. [40].

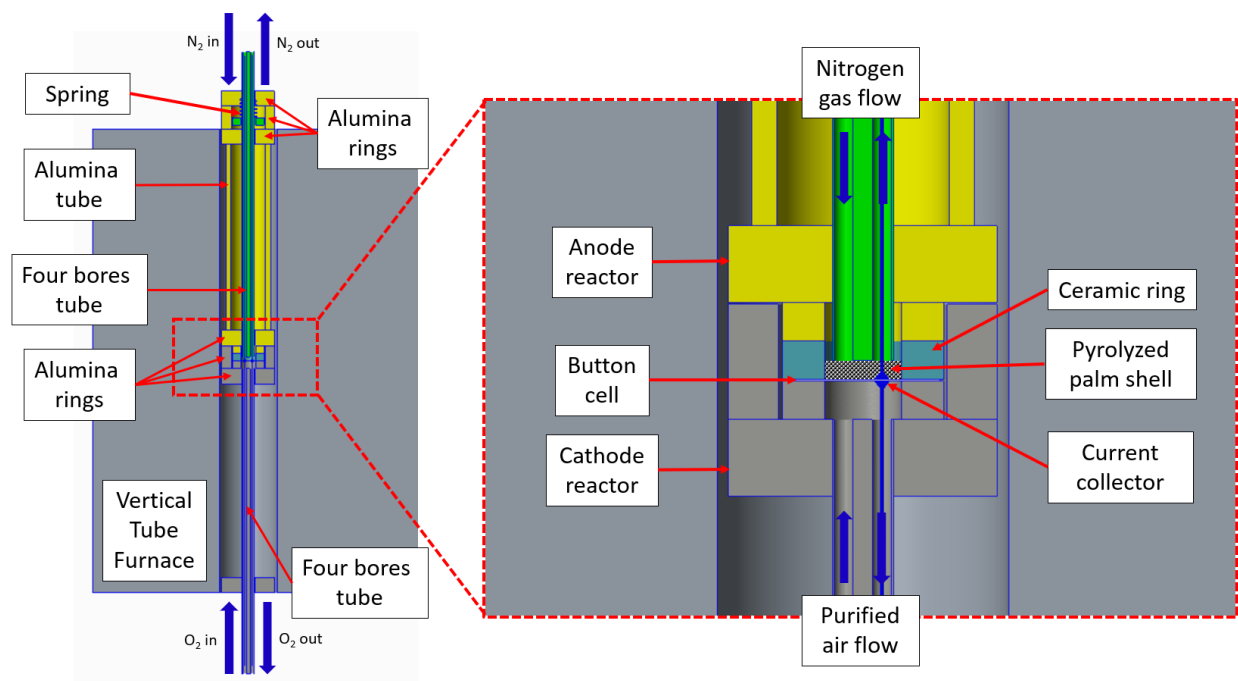


Figure 3.6: Cross section view of the DCFC reactor



### 3.3.3 Current collector

In this experiment, silver (Ag) and platinum (Pt) wires were used as current collector leads. Both wires used were 300 mm in length, 0.5 mm in diameter with 99.9 % purity. The Ag wires were supplied by Sigma-Aldrich while the Pt wires were supplied by KPL Scientific Inc.. The current collector leads were dipped into a concentrated Ag paste purchased from Sigma-Aldrich (>75 wt. % Ag powder) at 2 mm depth for 1 minute and was moved down to touch the surface of the cathode. Subsequently, the Ag paste was cured at 800 °C at 10 °C/min for 1 hour. Identical setup was repeated for Ag paste curing at the anode. The curing parameters were based on a comparison made by Gong Y.H. et al. [57] between Ag current collectors cured at 800 °C and 650 °C, respectively where the Ag current collector cured at 800 °C for 1 hour has shown the best DCFC performance. The current collector leads will be reused in the subsequent experiments after the leftover Ag paste on the wires was removed by using sandpaper. This is to ensure only the fresh Ag paste will be in contact with the current collector leads. Current collector leads with cured Ag paste on respective electrodes are shown in Figure 3.7 and Figure 3.8.



Figure 3.7: Cured Ag paste at Cathode



Figure 3.8: Cured Ag paste at Anode

The focus of Chapter 4 is to assess the effects of the material of the current collector lead on DCFC performance at 750 °C. Four different configurations were formulated and named Ag|Ag, Pt|Pt, Ag|Pt and Pt|Ag, respectively. For Ag|Ag, the single Ag wire was glued to anode and cathode surfaces respectively, whereas for Pt|Pt, single Pt wire was glued to both the electrode surfaces. As for Ag|Pt, single Ag wire was glued to anode surface while single Pt wire was glued to the cathode surface. In the case of Pt|Ag, the single Pt wire was glued to anode surface while single Ag wire was glued to the cathode surface. The wires were glued to the electrodes using Ag paste. Table 3.1 shows the configuration of the experiment setup studied in Chapter 4.

Table 3.1: Experiment setup to assess the impact of material of current collector to DCFC performance.

Experimental setup	Anode current collector lead	Cathode current collector lead	Current collection configuration	Temperature (°C)
Ag Ag	Single Ag wire	Single Ag wire	Point Ag paste	750
Pt Pt	Single Pt wire	Single Pt wire	Point Ag paste	750
Ag Pt	Single Ag wire	Single Pt wire	Point Ag paste	750
Pt Ag	Single Pt wire	Single Ag wire	Point Ag paste	750

Chapter 5 focused on the effects of quantity of current collector leads on the performance of DCFC. The number of current collector leads was varied on each side of the electrode as shown in Table 3.2. The numeral in front of Ag represents the quantity of the current collector leads used at the respective electrode.

Table 3.2: Experiment setup to evaluate the effect of number of current collector lead to the DCFC performance

<b>Experimental setup</b>	<b>Anode current collector lead</b>	<b>Cathode current collector lead</b>	<b>Current collection configuration</b>	<b>Temperature (°C)</b>
1Ag 1Ag	Single Ag wire	Single Ag wire	Point Ag paste	750
2Ag 1Ag	Double Ag wires	Single Ag wire	Point Ag paste	750
1Ag 2Ag	Single Ag wire	Double Ag wires	Point Ag paste	750
2Ag 2Ag	Double Ag wires	Double Ag wires	Point Ag paste	750

Chapter 6 studied the impact of the configurations of the current collection on the DCFC performance. For the Mesh-like paste type current collector, concentrated Ag paste (>75 wt. % Ag powder) was stirred for 1 minute and drawn on the electrodes surfaces in a mesh-like formation and cured at 800 °C for 1 hour in air. Subsequently, current collector leads were glued to both electrodes surfaces, and the rest of the setup employed were same as the first experiment. The experiment was repeated for Layer type current collector where the concentrated Ag paste (>75 wt. % Ag powder) was directly painted on to the entire electrodes surfaces. The experimental setup used in Chapter 6 can be found in Table 3.3.

Table 3.3: Experiment setup to evaluate the effect of configuration of current collector paste to the DCFC performance

<b>Experimental setup</b>	<b>Anode current collector lead</b>	<b>Cathode current collector lead</b>	<b>Current collection configuration</b>
Point	Double Ag wires	Double Ag wires	Point Ag paste
Mesh	Double Ag wires	Double Ag wires	Mesh-like Ag paste
Layer	Double Ag wires	Double Ag wires	Layer Ag paste

### 3.4 Operation of DCFC

Figure 3.9 shows the schematic of the DCFC reactor during operation. The button cell with current collector leads glued to its electrode surface was placed in the cathode reactor. After that, a ceramic ring (OD: 21 mm; ID: 10 mm) has been put on top of the button cell as shown in Figure 3.4. Then, 30 mg of pyrolyzed palm shells were loaded into the ceramic ring so that the pyrolyzed palm shells were contained within the anode. Subsequently, anode reactor was placed on top of the alumina ring. Current collector leads were connected to a potentiostat (Metrohm Autolab PGSTAT302N) via kelvin clips with a two-electrode method where Working (W) and Sense (S) leads are connected to the anode; while Counter (C) and Reference (R) leads are connected to the cathode. Nitrogen gas (99.999 %) was used as anode purge gas at 110 mL/min and 1.2 bars; while purified air was supplied to the cathode at 200 mL/min and 1 bar as oxidant gas. The higher pressure in anode compartment prevents gas from cathode compartment leaks into anode compartment. The DCFC was heated to 750 °C at 10 °C/min in a vertical tube furnace. When the temperature was stabilized, the electrical measurements were executed.

The operating temperature of 750 °C was chosen for the experiments due to the following reasons:

- i. YSZ requires operating temperature above 700 °C in order to have sufficient ionic conductivity [20].

ii. Severe evaporation of Ag was observed at 800 °C [34].

Hence, to ensure that sufficient ionic conductivity in YSZ without compromising the stability of Ag, 750 °C was chosen as the operating temperature of the experiments.

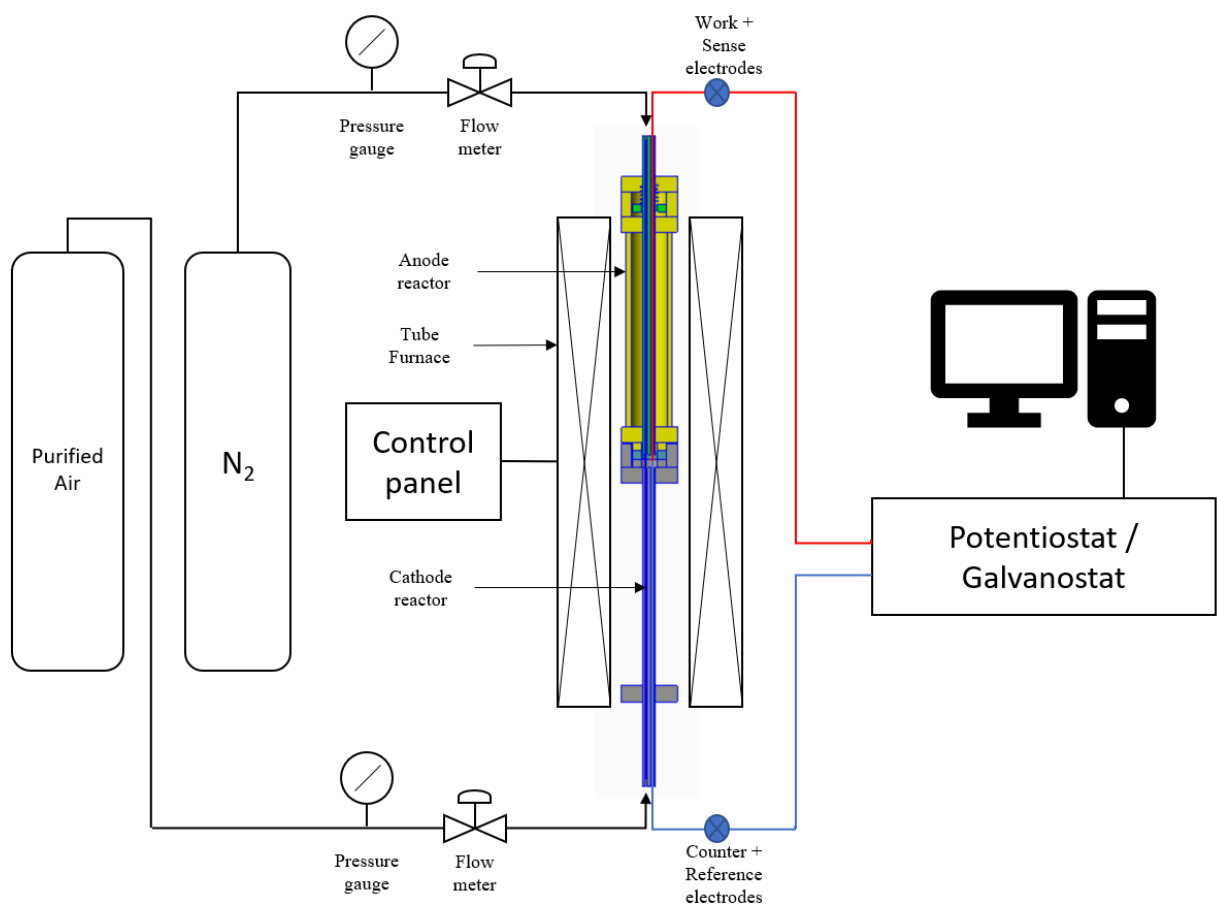


Figure 3.9: Schematic of DCFC system

### **3.5 Performance evaluation of DCFC**

The electrochemical characteristics of DCFC such as polarization curve and impedance were evaluated using LSV and EIS scan. The system was connected to potentiostat with two electrodes setting. Once the vertical tube furnace (Carbolite) reached 750 °C, the LSV scanning was commenced at a sweeping scan rate of 5 mV/s from OCV to 0 V, followed by the EIS scanning at a frequency range of 10 kHz to 0.1 Hz and excitation amplitude of 10 mV[36]. Frequency range was set to start at 10 kHz instead of 20 kHz to omit the inductance induced by wiring. The potential of the cells as a function of time was monitored with Chronopotentiometry (CP) with a constant loading of 1 mA for 1 hour to examine the carbon consumption rate of the experimental setup. Once CP measurements were done, LSV and EIS measurements were performed again. The Nyquist plots obtained in EIS measurements were simulated using Metrohm Autolab Nova 1.11.2 software.

## Chapter 4.

### Performance analysis of DCFC with platinum and silver current collector leads

#### 4.1 Overview

This chapter focuses on reporting the performance of DCFC affected by Platinum (Pt) and Silver (Ag) current collector leads used on its electrodes. The objective of this chapter is to study the current density, power density and impedance of the DCFC when coupled with Pt and Ag current collector leads. The current density and power density of the cells were measured with LSV method and depicted in V-I curves while the impedance of the cells was measured with EIS method and represented in Nyquist plot. The values of potential as a function of time of the cells was evaluated using Chronopotentiometry (CP) method. Also, the cost to performance ratio of current collector leads was included.

#### 4.2 Results and Discussions

Figure 4.1 and Figure 4.2 shows the performance curves of before and after CP measurement corresponding to Ag|Ag, Pt|Pt, Ag|Pt and Pt|Ag at 750 °C. Pt|Pt was served as control for the experiment. Before CP measurement, Ag|Ag exhibited highest current density and power density amongst other cells at 750 °C with the values of 21.1 mA/cm<sup>2</sup> and 7.3 mW/cm<sup>2</sup>; respectively. Followed closely are Pt|Ag and Ag|Pt with similar current density at the values of 17.2 mA/cm<sup>2</sup>. Despite having similar current density value, Pt|Ag exhibited slightly higher power density than Ag|Pt with the values of 6.0 mW/cm<sup>2</sup> and 5.2 mW/cm<sup>2</sup>; respectively. Pt|Pt displayed poorest current density and power density with the values of 14.2 mA/cm<sup>2</sup>.and 4.2 mW/cm<sup>2</sup>; respectively. The experimental OCV values were recorded at the range of 0.9 V, which is slightly lower than the theoretical OCV value which is 1.02 V[14]. This may be due to there was no

equilibrium established in the solid-solid contact or there was leakage in the system that caused the electrochemical activity of the carbon fuel lower than the ideal case such as submonolayers of active materials [40].

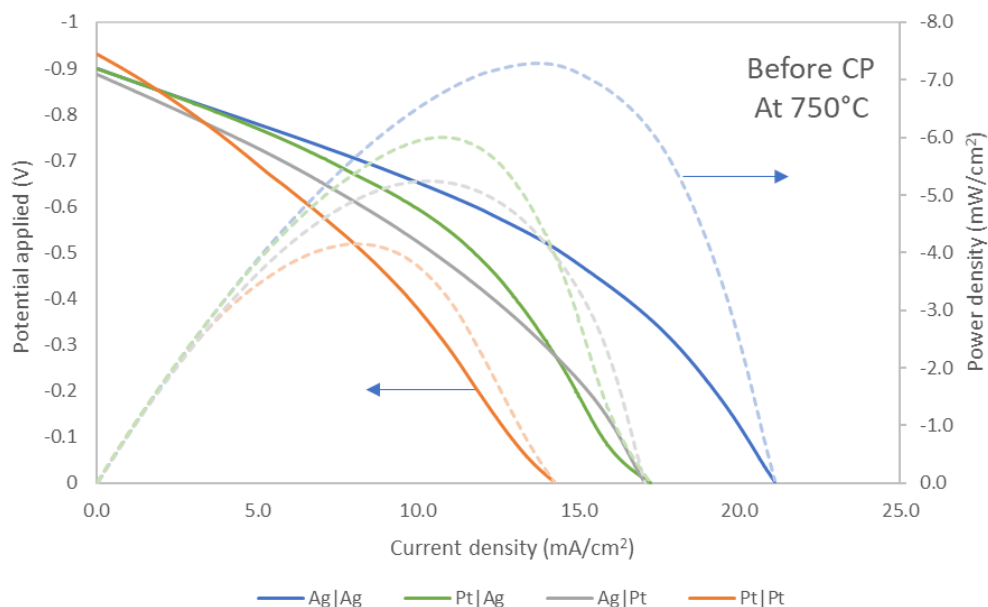


Figure 4.1: Performance curves of cells prior CP

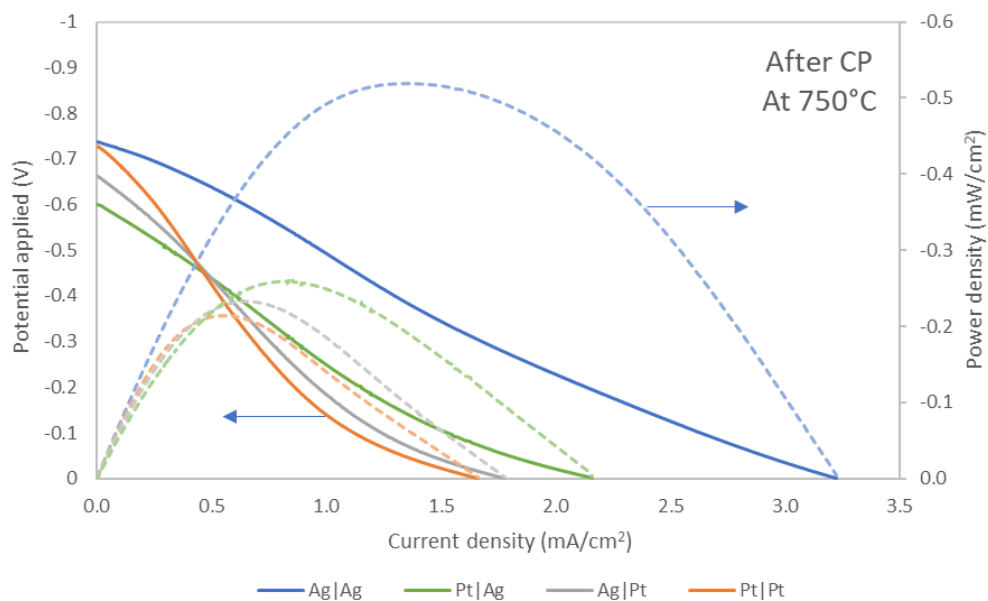


Figure 4.2: Performance curves of cells after CP



After CP measurement, the performance of the cells dropped significantly yet shared similar trend to the performance of the cells prior CP measurement. The performance of the cells was arranged in the following order of Ag|Ag, Pt|Ag, Ag|Pt and Pt|Pt. The values of performance curves of the cells were summarized in Table 4.1.

Table 4.1: Performance of cells corresponding to Ag|Ag, Pt|Ag, Ag|Pt and Pt|Pt prior and after CP measurements

	Before CP		After CP	
	$I_{\max}$ (mA/cm <sup>2</sup> )	$P_{\max}$ (mW/cm <sup>2</sup> )	$I_{\max}$ (mA/cm <sup>2</sup> )	$P_{\max}$ (mW/cm <sup>2</sup> )
Ag Ag	21.1	7.3	3.2	0.52
Pt Ag	17.2	6	2.2	0.26
Ag Pt	17.2	5.2	1.8	0.23
Pt Pt	14.2	4.2	1.6	0.21

Figure 4.3 and Figure 4.4 display area-corrected Nyquist plots of before and after CP measurement corresponding to cells employing different current collectors at 750 °C. The Nyquist plots were measured using EIS method once the value of Open Circuit Voltage (OCV) have been stabilized after LSV measurements. Equivalent circuits illustrated in Figure 4.5 fitted reasonably well with the Nyquist plots (without area correction of 0.79 cm<sup>2</sup>) with the goodness of fit or chi-squared ( $\chi^2$ ) values being 10<sup>-3</sup>.

The impedance started with high-frequency which was denoted as 10 kHz and ended with low-frequency which was denoted as 0.1 Hz as shown in Figure 4.3. The value where high-frequency arc intersected with real impedance axis  $Z'$  was called ohmic resistance and was represented by  $R_{\text{ohmic}}$ .  $R_{\text{ohmic}}$  was attributed by two major resistances. The first one was electrical

resistances of the current collector, electrodes, and electrolyte. The second major resistance was the contact resistances between current collector, electrodes, and fuels.

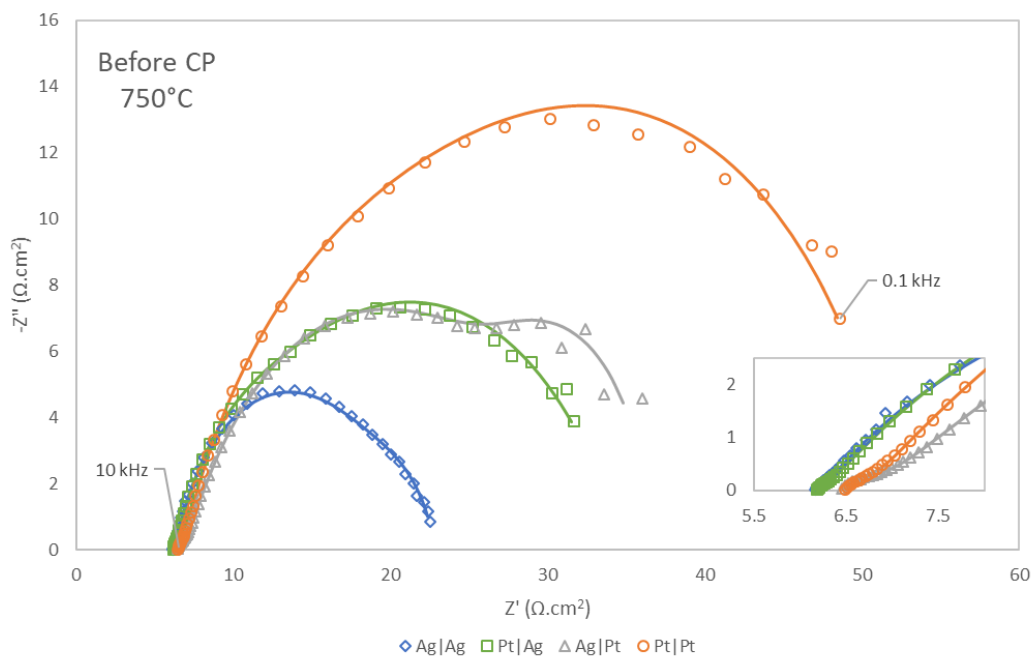


Figure 4.3: Nyquist plots of cells before CP. The inset shows the close-up look of the Nyquist plots.

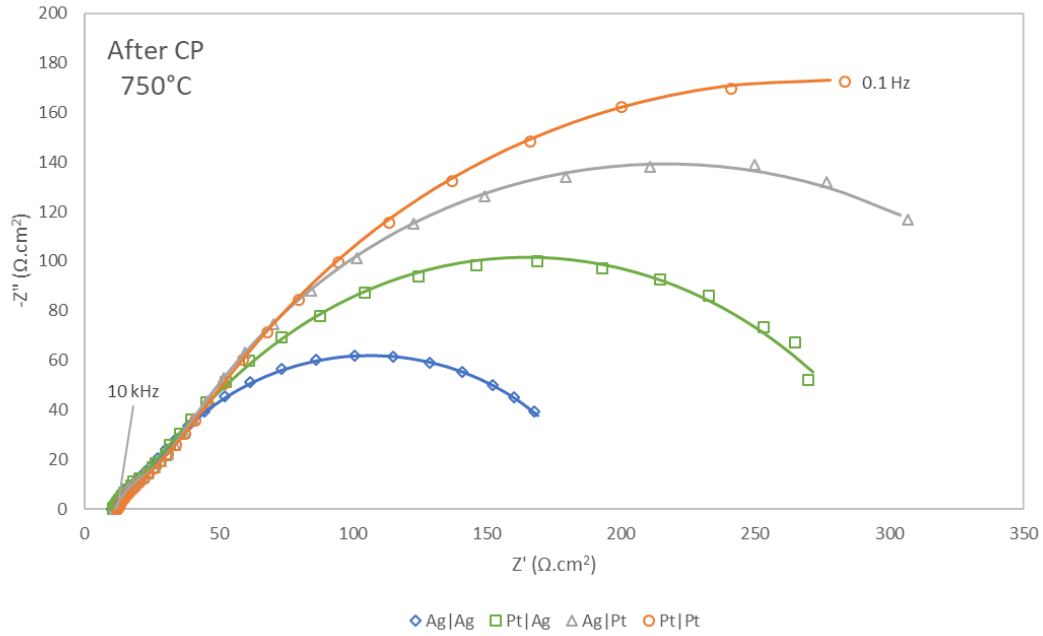


Figure 4.4: Nyquist plots of cells after CP. The inset shows the close-up look of the Nyquist plots.

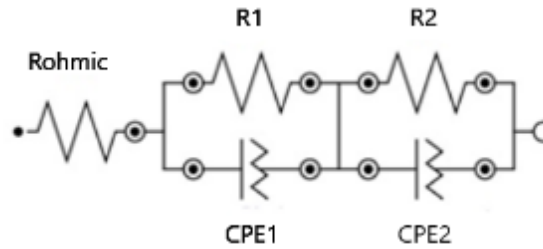


Figure 4.5: Equivalent circuit used for fitting Nyquist plot

The high-frequency arc represents electrochemical oxidation of carbon at the interface of current collector/anode and anode/electrolyte which denoted by the parallel joint of R1 and CPE1 [8, 37] where R1 denotes charge transfer resistance of carbon oxidation at anode and CPE denotes constant phase element which is the electrical capacitance double layer. Meanwhile, the low-frequency arc corresponds to mass diffusion process [84] where electrochemical oxidation of CO happens at the interface of current collector/anode and anode/electrolyte was symbolized as a

parallel joint of R2 and CPE2 [8]. R2 represents the charge transfer resistance of CO oxidation at anode. The values of  $R_{ohmic}$ , R1, R2, and  $R_{total}$  are summarized in Table 4.2.

Table 4.2: Values of resistors by fitting equivalent circuit (Figure 4.5) into Nyquist plots (Figure 4.3 and Figure 4.4)

	Before CP ( $\Omega.cm^2$ )				After CP ( $\Omega.cm^2$ )			
	$R_{ohmic}$	R1	R2	$R_{total}$	$R_{ohmic}$	R1	R2	$R_{total}$
Ag Ag	6.1	0.2	16.5	22.9	10.1	1.5	182.5	194.1
Pt Ag	6.2	0.3	28.5	35.0	10.3	1.6	305.7	317.6
Ag Pt	6.4	0.5	29.8	36.7	11.1	1.8	396.8	409.8
Pt Pt	6.5	0.6	46.1	53.2	11.9	1.8	501.4	515.2

From Table 4.2, the trend of the Nyquist plots of before CP and after CP was similar and it was arranged in the order of Ag|Ag > Pt|Ag > Ag|Pt and Pt|Pt. Ag|Ag has the lowest  $R_{ohmic}$  and  $R_{total}$  when compared to the other cells. Next, Pt|Ag has a slightly higher  $R_{ohmic}$  relatively to Ag|Ag albeit with a higher  $R_{total}$ . Followed up closely was Ag|Pt with high  $R_{ohmic}$  yet slightly higher  $R_{total}$  than Pt|Ag. Finally, Pt|Pt has the highest  $R_{ohmic}$  and  $R_{total}$  of all the cells.

Potential values displayed in Figure 4.6 were shown to change as a function of time at 750 °C. The potential decreased steadily but with different rate corresponding the materials used as current collector leads. The potential of Ag|Ag decreased by 0.44 V/hr, followed by Pt|Ag with the potential dropped at the rate of 0.65 V/hr. Both Ag|Pt and Pt|Pt displayed similar potential drop rate with the values of 0.72 V/hr and 0.73 V/hr; respectively.

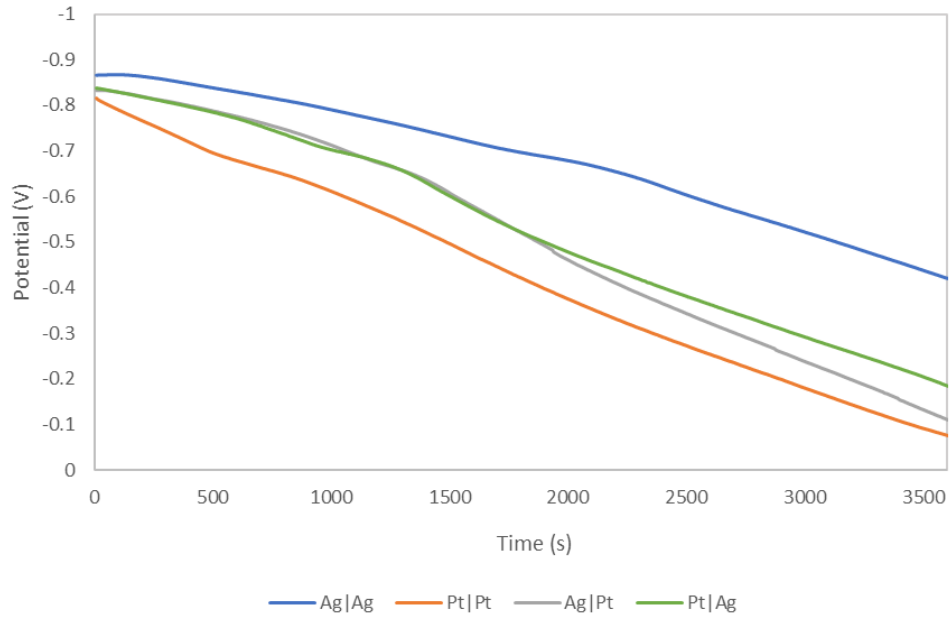


Figure 4.6: Potential as a function of time at 750 °C

In connection with the results in Table 4.1, Table 4.2 and Figure 4.6, the values of  $R_{\text{total}}$  of cells were inversely proportional with the performances of the cells which were contributed by the electrochemical reactions shown in reaction (1), (2), (3) and (4)[6]:



Amongst the cells, Ag|Ag has the lowest  $R_{\text{total}}$  prior to and after CP measurement. Since cells were tested with same setup and same amount of palm shell, the contribution from contact resistance between palm shell, electrodes and current collector leads were minimal. Therefore, the performance differences between the cells were most likely contributed by the electrical resistivity of the material used in the cells. It was evident that the usage of Ag current collector leads which has the lowest electrical resistance at 72 nΩ.m [85] on both of Ag|Ag electrodes has caused the

low value of  $R_{ohmic}$ . The low electrical resistance of Ag has enabled higher rate of electrons flowing into cathode which has accelerated the rate of oxygen reduction and resulted in higher production rate of oxygen ions. Subsequently, high amount of CO was produced at higher rate when high amount of oxygen ions reacted with palm shells available at anode via reaction (2). The produced CO will interact with large portion of anode which was made of nickel oxide (NiO) and reduced it into nickel (Ni) via reaction (5) [86]. The reduced NiO peaks and prominent Ni peaks shown by reacted button cell in XRD results have proven that NiO in the button cell has reduced to Ni in Figure 4.7. As Ni has lower resistance than NiO, the material resistance of the anode reduced substantially, which contributed to the low  $R_{ohmic}$  of Ag|Ag.

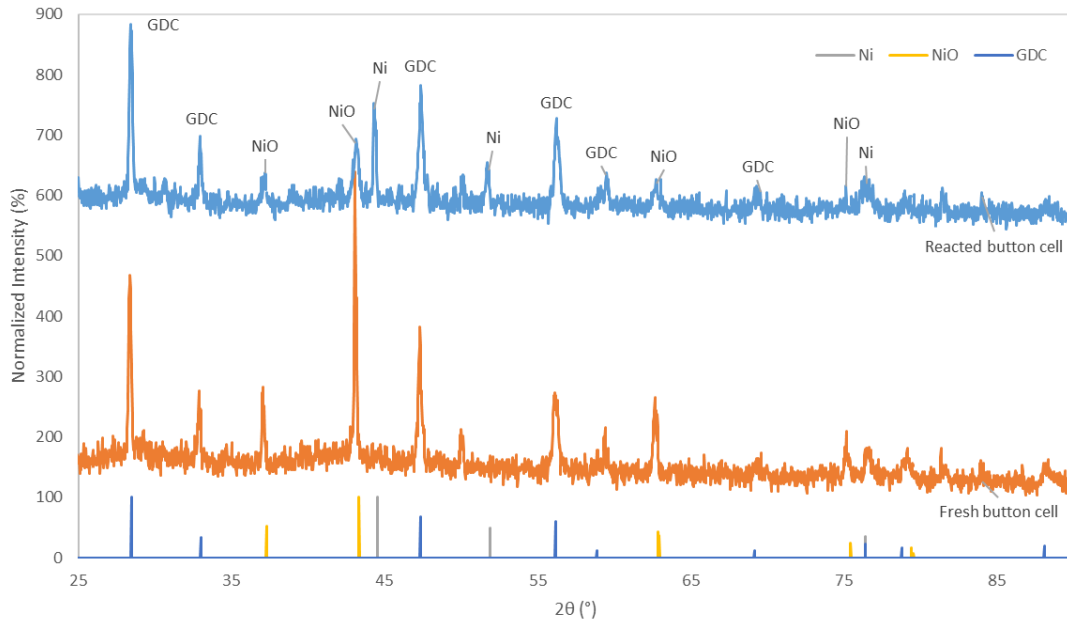


Figure 4.7: XRD results of fresh button cell and reacted button cell

Since Ag current collector lead was used at anode, the high number of generated electrons via reaction (2), (3) flowed out of anode without restriction, resulting in low  $R_1$  value of Ag|Ag shown in Table 4.1. The produced CO via reaction (3) then diffused into the reduced anode which has

plenty of porosities for gas diffusion and reacted with the plentiful oxygen ions available at the interface of anode and electrolyte via reaction (4). A high number of electrons produced via reaction (4) flowed out of anode without limitation through Ag current collector lead which was reflected in the low  $R_2$  value of Ag|Ag shown in Table 4.1. Consequently, high current density and power density were observed in Ag|Ag.

Prior to CP measurement, Pt|Ag and Ag|Pt shared similar  $R_{total}$  albeit relatively greater than Ag|Ag due to the usage of Pt current collector lead which has high electrical resistance of 385  $n\Omega.m$  [87]. The similarity of  $R_{total}$  for both cells explained the reason both cells have similar current density. Both cells used Ag and Pt current collector leads in their setup. However, Pt|Ag exhibited  $R_{ohmic}$  lower than Ag|Pt due to the usage of Ag current collector leads at cathode which influenced the reduction stage of anode. As such,  $R_{ohmic}$  was observed to be largely affected by the material of current collector lead used in cathode and the stage of reduction of anode. The usage of Ag current collector lead at the cathode of Pt|Ag has caused the rate of electrons entering cathode unrestricted which has accelerated the rate of oxygen ions produced through oxygen reduction reaction. Therefore, higher rate of carbon oxidation at anode via reaction (2), (3) and (4) has enhanced the generation of electrons at anode. Nevertheless, the usage of Pt current collector lead at anode has restricted the rate of electron flowing out of anode. As a result,  $R_1$  and  $R_2$  value of Pt|Ag which were slightly higher to Ag|Ag as shown in Table 4.1 were observed. The huge difference of electrons availability at cathode and anode for Pt|Ag has generated high voltage within the cell, ensuing in higher power density than Ag|Pt.

In contrary, Ag|Pt uses Pt current collector lead at its cathode. Therefore, the rate of electrons entering cathode for oxygen reduction reaction has been constrained and impacted the generation rate of oxygen ions. As such, the lowered rate of carbon oxidation has affected the

production of CO and electrons at anode and limited the reduction stage of anode. The reduced porosities of anode have imparted the diffusion process of CO for further oxidation into CO<sub>2</sub>. The usage of Ag current collector lead at anode has ease electrons flowing out of anode. However, it does not help in reducing the R1 and R2 values as the production of oxygen ions at cathode were the limiting factor. The voltage of Ag|Pt was low due to the small difference of electrons availability at cathode and anode. Hence, the power density generated by Ag|Pt was not as high as Pt|Ag.

Nevertheless, the gap between Pt|Ag and Ag|Pt especially on  $R_{total}$  has widened to 116.7  $\Omega$  after CP measurement as shown in Table 4.2. The huge differences of  $R_{total}$  were dominantly contributed by R2 values of both cells which were related to diffusion process of CO into anode for further oxidation. A plausible explanation for the widening gap was that the state of anode being maintained in Ni was different for both cells. Pt|Ag has most of the anode maintained in Ni state due to high carbon oxidation rate with the usage of Ag on cathode. The high carbon oxidation rate has prevented the accumulation of oxygen ions at the interface of anode and electrolyte that will re-oxidized Ni into NiO. In contrast, Ag|Pt has fewer of the anode preserved in Ni state due to the sluggish carbon oxidation rate with the usage of Pt on cathode. The slow carbon oxidation has generated lesser CO to maintain anode in Ni state, inducing higher rate of re-oxidation of Ni to NiO that has reduced the porosities in the anode. Hence, it was difficult for CO to diffuse into anode for further oxidation into CO<sub>2</sub> which has reflected in the high R2 value after CP measurement for Ag|Pt.

Pt|Pt has displayed the worst performance amongst the cells due to the usage of Pt current collectors at both of its electrodes which were reflected by the highest  $R_{total}$  value and  $R_{ohmic}$  value in Table 4.1. The high electrical resistance of Pt current collector leads at cathode has capped the



rate of electrons entering cathode. Therefore, the production of oxygen ions at cathode which eventually used in carbon oxidation at anode has been restricted. The restricted carbon oxidation has resulted in a slower rate of CO and electrons generation which caused lesser area of anode being reduced to Ni. The reduced porosities of anode have impeded the diffusion process of CO into anode for further oxidation. Coupled with the usage of Pt current collector lead at anode, the rate of electrons flowing out of anode through Pt current collector lead has decreased, resulting in high R1 and R2 values for Pt|Pt. The limited flow of electrons in Pt|Pt has caused low current density and power density as observed in Figure 4.1. The change of trend according to the electrical conductivity of the material used as current collector leads at cathode signifies that oxygen reduction process at cathode might play a dominant role in overall DCFC performance than the carbon oxidation process at anode.

During CP measurement for 1 hour duration, the pyrolyzed palm shells were continuously oxidized at the interface of anode and current collector, leaving lesser pyrolyzed palm shell and more ashes on the surface of anode. The accumulation of ashes which is a poor electrical conductor, has impeded the electrochemical reaction of carbon oxidation, which explains the trend of significant drop in maximum power density, current density and  $R_{total}$  after CP measurement. The potential of the cell was affected also by CP measurement as shown in the Figure 4.6. Ag|Ag and Pt|Ag current collector leads have higher potential than Ag|Pt and Pt|Pt current collector leads at the end of CP. Based on Nernst equation shown below, the potential values were affected by the oxygen activity.

$$E = E^0 - \frac{RT}{nF} \ln \left( \frac{a_{O_2,c}}{a_{O_2,a}} \right)$$

$a_{O_2,c}$  and  $a_{O_2,a}$  are oxygen activity on cathode and anode, respectively. Cells with high potential value have low anodic oxygen activity due to high oxidation rate while cell with low potential

value has high anodic oxygen activity due to sluggish oxidation rate [79, 86]. This indicates that cells with Ag|Ag and Pt|Ag current collector leads have low anodic oxygen activity due to higher oxidation rate of palm shell into CO. As both cells used Ag current collector at cathode, it has demonstrated that high electronic conductivity of Ag current collector lead at cathode has unrestricted the electron to flow to cathode for oxygen reduction, hence explained the high rate of carbon oxidation. In contrast, cells with Ag|Pt and Pt|Pt current collectors have lower potential at the end of CP due to high anodic oxygen activity caused by sluggish carbon oxidation rate. As both cells used Pt current collector at cathode, the low electronic conductivity of Pt has restricted the electron flow to cathode for oxygen reduction, hence reducing the number of oxygen ions that will flow to anode. As a result, the rate of carbon oxidation was low. The change of trend corresponding to the electronic conductivity of the material used as current collector leads at cathode signifies that oxygen reduction process at cathode was a limiting factor in overall DCFC performance than the carbon oxidation process at anode.

The price to performance ratio of Ag|Ag, Pt|Ag, Ag|Pt and Pt|Pt at 750 °C in this experiment was calculated as follows:

Length of wire used in experiments: 0.3 m

The price of a Ag wire reel sold by Sigma-Aldrich: USD 168 per meter

The price of a Pt wire reel sold by Sigma-Aldrich: USD 1525 per meter

Ag|Ag

The maximum power density: 7.3 mW.cm<sup>-2</sup>

Price to performance ratio =  $2 * (\text{USD } 168 * 0.3) / 7.3 \text{ mW.cm}^{-2} = \text{USD } 13.8 / \text{mW.cm}^{-2}$

Pt|Ag

The maximum power density: 6.0 mW.cm<sup>-2</sup>

Price to performance ratio =  $[(\text{USD } 1525 * 0.3) + (\text{USD } 168 * 0.3)] / 6.0 \text{ mW.cm}^{-2} = \text{USD } 84.7 / \text{mW.cm}^{-2}$

Ag|Pt

The maximum power density: 5.2 mW.cm<sup>-2</sup>

$$\text{Price to performance ratio} = [(\text{USD } 168 * 0.3) + (\text{USD } 1525 * 0.3)] / 5.2 \text{ mW.cm}^{-2} = \text{USD } 97.7 / \text{mW.cm}^{-2}$$

#### Pt|Pt

The maximum power density:  $4.2 \text{ mW.cm}^{-2}$

$$\text{Price to performance ratio} = 2 * (\text{USD } 1525 * 0.3) / 4.2 \text{ mW.cm}^{-2} = \text{USD } 217.9 / \text{mW.cm}^{-2}$$

Based on the results of this study, it appeared that Ag|Ag was the best current collector choice for measuring the performance of DCFC considering it has 15 times lesser of price to performance ratio compared to Pt|Pt.

### **4.3 Conclusions**

The effects of the material of current collector leads on DCFC performance were studied. It was apparent that DCFC exhibits significant disparity in performance depending on the type of current collector used. At  $750^\circ\text{C}$ , Ag|Ag current collector leads has the best DCFC performance whereas Pt|Pt current collector leads has the worst DCFC performance. It is well known that sluggish kinetics of carbon oxidation at anode limits the DCFC performance. However, in this experiment, the electrical resistance of the material used as current collector lead especially at cathode plays a vital role in determining the overall DCFC performance. Cells with Ag current collector leads at the cathode have shown to have higher current density, higher power density, and lower total resistance than the cells with Pt current collector leads at cathode. This implies that to determine the kinetic rate of carbon oxidation at anode accurately, oxygen reduction process at cathode has to be properly studied as it has influence on the overall performance of DCFC. As an effort to reduce operation cost of DCFC, DCFC operates at  $750^\circ\text{C}$  with Ag|Ag current collector leads was selected for further optimization in the next section due to its low price to performance ratio. The overall performance of DCFC at  $750^\circ\text{C}$  will be enhanced by various means such as

adding additional Ag current collector leads to the cells or applying an additional layer of Ag paste on the cathode which cost only a fraction of the cost for additional Pt current collector leads.

## **Chapter 5.**

### **Performance analysis of DCFC with varied number of current collector leads**

#### **5.1 Overview**

The trend of maximum current density compiled from the literature listed in Table 2.3 deviates from the conclusion made by Jiang, S.P. where the cell impedance should be inverse proportional with contact area. The cause of this performance deviations is mainly caused by different type of fuels, active area of electrode and material of current collector used in the literature. Therefore, in this chapter, the performance of DCFC with various number of current collector leads used on its electrodes was observed and analyzed while the DCFC setup and other operating parameters were controlled to minimize the interference to the performance of DCFC. The objective of this chapter is to study the current density, power density and impedance of the DCFC when coupled with single or double current collector leads. The current density and power density of the cells exhibited in V-I curves were measured with LSV method while the impedance of the cells displayed in Nyquist plot was measured with EIS method.

#### **5.2 Results and Discussions**

Data of Ag|Ag was used as a benchmark for this experiment, and it was denoted as 1Ag|1Ag from here onwards. Figure 5.1 illustrates V-I curves of 1Ag|1Ag, 1Ag|2Ag, 2Ag|1Ag, and 2Ag|2Ag measured using LSV method.

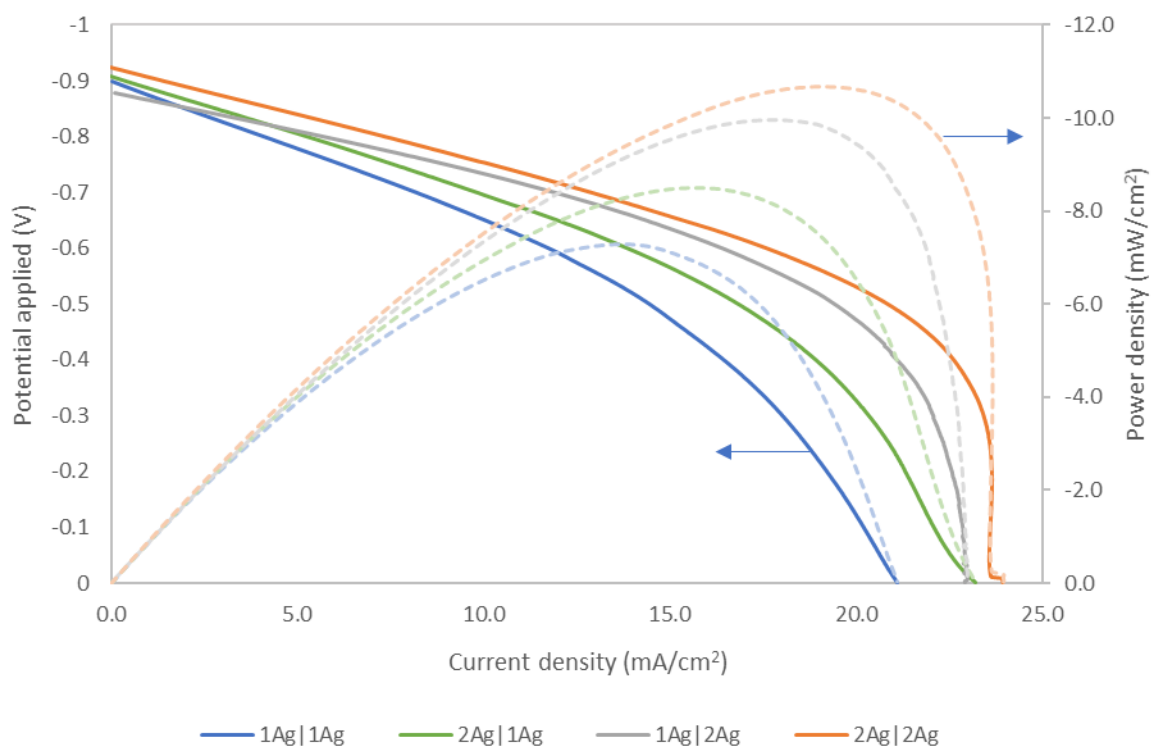


Figure 5.1: V-I curves of cells with 1Ag|1Ag, 1Ag|2Ag, 2Ag|1Ag, and 2Ag|2Ag current collector leads at 750 °C

As shown in Figure 5.1, the best cell performance was obtained from the cell with 2Ag|2Ag current collector leads, which has current density of 23.9 mA/cm<sup>2</sup> and power density of 10.7 mW/cm<sup>2</sup>. Follow up closely were the cell with 1Ag|2Ag current collector leads at 23.0 mA/cm<sup>2</sup> and 10.0 mW/cm<sup>2</sup> and cell with 2Ag|1Ag current collector leads at 22.8 mA/cm<sup>2</sup> and 8.5 mW/cm<sup>2</sup>. Cell with 1Ag|1Ag current collector leads has least current density and power density at 21.1 mA/cm<sup>2</sup> and 7.3 mW/cm<sup>2</sup>; respectively. The values of each cells were summarized in Table 5.1. The noticeable differences in max current densities and peak power densities of the cells with additional current collector leads at cathode and anode indicated that the performance of the cell was also influenced by the number of current collection leads.

Table 5.1: Performance of cells corresponding to 1Ag|1Ag, 2Ag|1Ag, 1Ag|2Ag and 2Ag|2Ag

	$I_{\max}$ (mA/cm <sup>2</sup> )	$P_{\max}$ (mW/cm <sup>2</sup> )
1Ag 1Ag	21.1	7.3
2Ag 1Ag	22.8	8.5
1Ag 2Ag	23.0	10.0
2Ag 2Ag	23.9	10.7

Figure 5.2 depicts Nyquist plots of cells using a different number of current collector leads at respective electrodes at 750 °C. The cells were monitored via EIS measurements once LSV measurements have been completed and OCV values have stabilized. Equivalent circuits illustrated in Figure 4.5 fitted reasonably well with Nyquist plots shown in Figure 5.2 with the goodness of fit or chi-squared ( $\chi^2$ ) values being  $10^{-3}$ . Table 5.1 summarizes the values of  $R_{\text{ohmic}}$ ,  $R_1$ ,  $R_2$  and  $R_{\text{total}}$ .

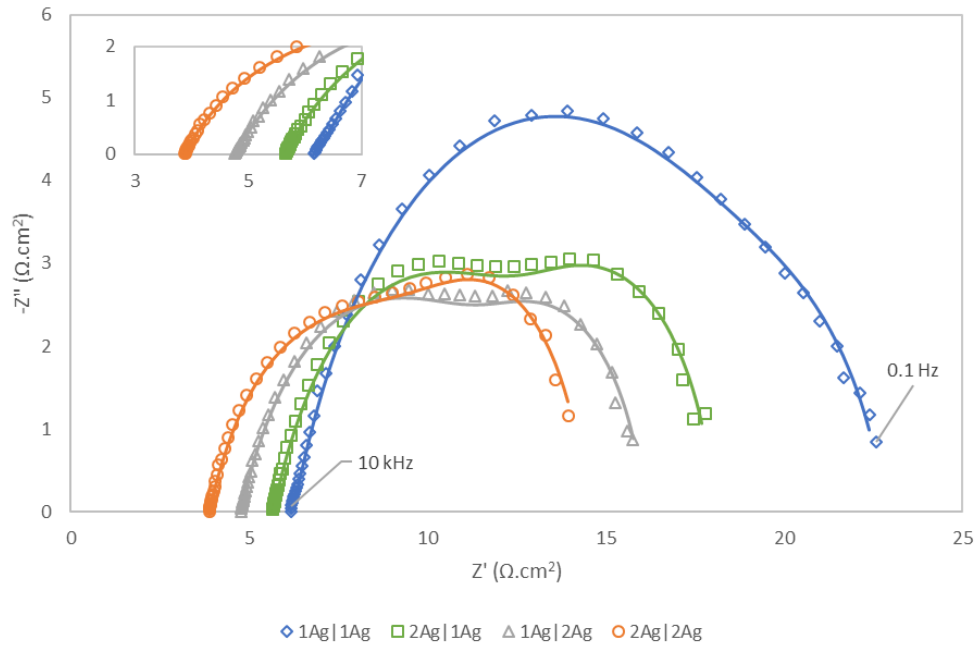


Figure 5.2: Nyquist plot of cells with 1Ag|1Ag, 2Ag|1Ag, 1Ag|2Ag and 2Ag|2Ag current collectors at 750 °C. The inset shows the close-up look of the Nyquist plots.

From Table 5.2, 2Ag|2Ag has yielded the lowest  $R_{ohmic}$  and  $R_{total}$  amongst other cells. Next, 1Ag|2Ag has a higher  $R_{ohmic}$  and  $R_{total}$  relatively to 2Ag|2Ag. Followed up closely was 2Ag|1Ag which possesses higher  $R_{ohmic}$  than 1Ag|2Ag yet offers similar  $R_{total}$  with 1Ag|2Ag. Finally, 1Ag|1Ag has the highest  $R_{ohmic}$  and  $R_{total}$  of all the cells. Relating to the results in Figure 5.1, Figure 5.2 and Table 5.1, the performance of DCFC benefited from the installation of additional current collector lead at electrodes.

Table 5.2: Values of resistors by fitting equivalent circuit (Figure 4.5) into Nyquist plot (Figure 5.2)

	$R_{ohmic}$	$R_1$	$R_2$	$R_{total}$
1Ag 1Ag	6.1	0.2	16.5	22.8
2Ag 1Ag	5.7	0.2	11.2	17.0
1Ag 2Ag	4.7	0.2	12.0	16.9
2Ag 2Ag	3.9	0.1	10.7	14.6

The installation of additional current collector lead at cathode of 2Ag|2Ag has doubled up the contact area between cathode and current collector leads, thus reducing the contact resistance of the cell while increasing the rate of electron entering cathode for oxygen reduction reaction. The increasing rate of electron was reflected as high current density in Figure 5.1. Its excellent oxygen reduction at cathode has enhanced the rate of oxygen ions entering anode, which indirectly influenced carbon oxidation at anode, producing high amount of CO and electrons which were shown as low  $R_1$  value for 2Ag|2Ag. As a result, a significant portion of anode has been reduced to Ni after reacting with reducing gas CO, which was reflected in the low  $R_{ohmic}$  because Ni has lower electrical resistance compared to NiO. The particle size of NiO shrank when it was reduced to Ni, thus creating high amount of porosities in the anode which was proven by Malzbender et al. [88]. The high amount of porosities in anode has eased the diffusion of CO for subsequent



oxidation into  $\text{CO}_2$ . The installation of additional current collector lead at anode has enlarged the contact area between anode and current collector lead while shortening the traveling path of generated electrons from leaving anode. Therefore, low value of  $R_1$  and  $R_2$  were observed for  $2\text{Ag}|2\text{Ag}$  which translated to the high current density and power density illustrated by  $2\text{Ag}|2\text{Ag}$ . A sharp drop of cell potential as the limiting current is approached was observed. The observed behavior has been associated to accumulation of CO at the anode followed by fuel starvation at high current densities as discussed by A.C. Rady et al.[7]. CO is consumed at a higher rate than the rate it can be supplied to anode during higher forced cell loading. Thus, higher currents cannot be sustained by CO, leading to a drop in current for subsequent voltage once CO is depleted. Figure 5.3 displays the flow of electrons and oxygen ions in  $2\text{Ag}|2\text{Ag}$ .

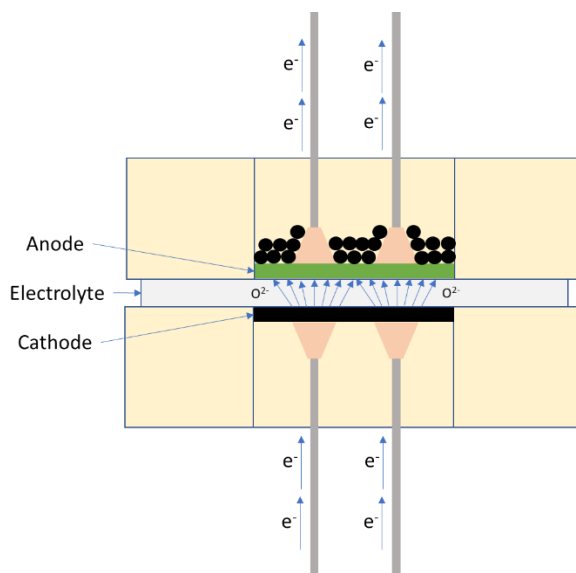


Figure 5.3: Schematic shows the flows of electrons and oxygen ions in  $2\text{Ag}|2\text{Ag}$

$1\text{Ag}|2\text{Ag}$  has exhibited DCFC performance that was superior to  $1\text{Ag}|1\text{Ag}$  due to the advantage it holds by having extra current collector lead installed to its cathode. The installation of additional current collector lead at cathode has allowed higher rate of electrons to flow to cathode for oxygen reduction. Thus palm shell at anode has gained more access to oxygen ions,

contributing to higher rate of carbon oxidation and eventually leading to high amount of CO and electrons. The high amount of CO ensures that majority area of the anode has been reduced to Ni, aiding diffusion process of CO into anode for further oxidation. Nevertheless, the usage of single current collector lead at anode has resulted in higher contact resistance at anode which can be seen in the slightly higher  $R_{ohmic}$  of 1Ag|2Ag when compared to 2Ag|2Ag. Therefore, the traveling pathway of electrons leaving anode for 1Ag|2Ag was longer than 2Ag|2Ag, which was detrimental to the rate of electrons leaving anode and thus explained the higher R1 and R2 values of 1Ag|2Ag. The high total resistance of 1Ag|2Ag compared to 2Ag|2Ag has resulted in generation of lower current density and power density. Figure 5.4 shows the flow of electrons and oxygen ions of 1Ag|2Ag.

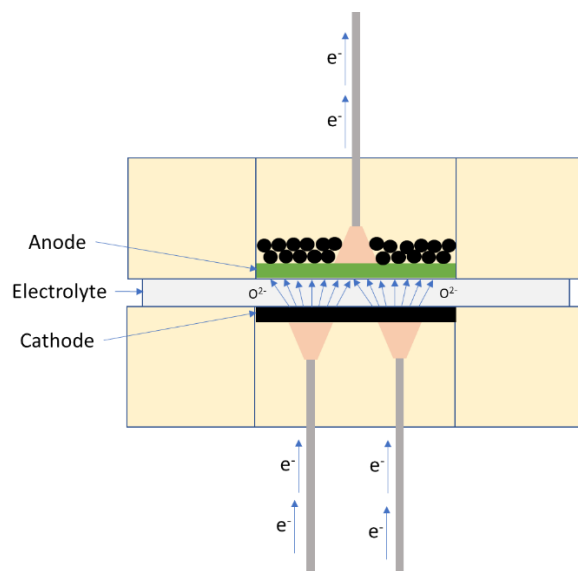


Figure 5.4: Schematic depicting the flow of electrons and oxygen ions in 1Ag|2Ag

Meanwhile, the inclusion of extra current collector lead at anode as shown by 2Ag|1Ag has displayed an improvement in performance relative to 1Ag|1Ag in terms of current density, power density, and total resistance. The rate of oxygen reduction at the cathode of 2Ag|1Ag should be similar to 1Ag|1Ag as both cells have single current collector lead glued to their cathodes.

Likewise, the amount of surface of anode reduced to Ni for both cells should be matching as well because the rate of the carbon oxidation for both cells were identical. Nevertheless, the inclusion of extra current collector lead at anode for 2Ag|1Ag has enhanced the contact area between current collector leads and anode which has resulted in slightly lower  $R_{ohmic}$  for 2Ag|1Ag relatively to 1Ag|1Ag. Besides that, the shortened travel distance of electron generated from carbon oxidation as shown in Figure 5.5 has caused in the lower R1 and R2 value. As a result, 2Ag|1Ag has possessed higher current density and power density relative to 1Ag|1Ag.

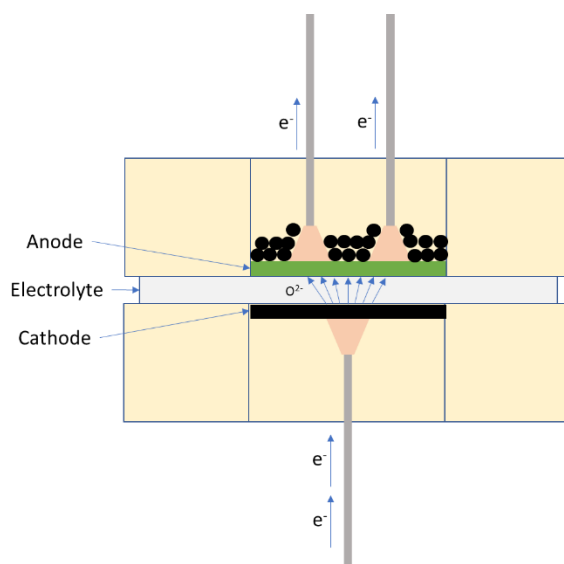


Figure 5.5: Schematic depicting the flow of oxygen ions and electrons in 2Ag|1Ag

Despite having similar current density and total resistance between 1Ag|2Ag and 2Ag|1Ag, 1Ag|2Ag was superior to 2Ag|1Ag in peak power density. A plausible explanation for this observation was that the availability of electrons at the electrodes of both cells was different. The electrons of 1Ag|2Ag were entering cathode at a rate that was doubled the rate of electrons entering cathode for 2Ag|1Ag. However, the usage of single current collector lead at the anode of 1Ag|2Ag has capped the rate of electrons leaving anode. As such, the voltage of 1Ag|2Ag was high, ensuring high power density due to the huge difference of electrons available at respective electrodes.

Whereas for 2Ag|1Ag, the rate of electrons entering the cathode was low. Coupled with double current collector leads at anode which enhanced the rate of electrons leaving the anode, the difference of electrons at anode and cathode of 2Ag|1Ag was small. Hence, the voltage of 2Ag|1Ag was low, which translated to lower power density than 1Ag|2Ag. The trend observed between 1Ag|2Ag and 2Ag|1Ag indicates that the power density of a cell was largely affected by the cathode of the cell.

### **5.3 Conclusions**

The effects of number of current collector leads and configurations of current collector on DCFC performance were studied. At 750 °C, the DCFC performance in terms of current density and total resistance was observed to increase proportionally with the number of current collector leads regardless of which electrode they were attached to. However, the peak power density was largely enhanced by additional current collector leads attached to cathode as shown by 1Ag|2Ag and 2Ag|2Ag cells due to the increased rate of oxygen reduction at cathode which subsequently boosted the rate of carbon oxidation. This implies that the reactions at cathode hold similar influence as the reactions at anode in determining the performance of DCFC.

## **Chapter 6.**

### **Performance analysis of DCFC with different configurations of current collector**

#### **6.1 Overview**

Current collector serves as a network for the electrons produced from electrochemical reactions at the anode to move to the cathode for oxygen reduction process. Hence, the configuration of the current collector will affect the DCFC performance, and it is important to understand the working mechanism. In this chapter, the performance of DCFC with various configuration of current collector used attached to its electrodes was observed and analyzed while the DCFC setup and other operating parameters were controlled to minimize the interference to the performance of DCFC. The objective of this chapter is to study the impact of point paste, mesh-like paste and layer paste current collector to DCFC performance by analyzing the current density, power density and impedance of DCFC. The current density and power density of the cells shown in V-I curves will be measured with Linear Sweep Voltammetry method while the impedance of the cells illustrated in Nyquist plot will be measured with EIS method.

#### **6.2 Results and Discussions**

The data of 2Ag|2Ag was used as a benchmark for this experiment and here in referring as Point type current collector. The effect of point type, mesh type and layer type current collector to the DCFC performance at 750 °C were portrayed in Figure 6.1 and Figure 6.2.

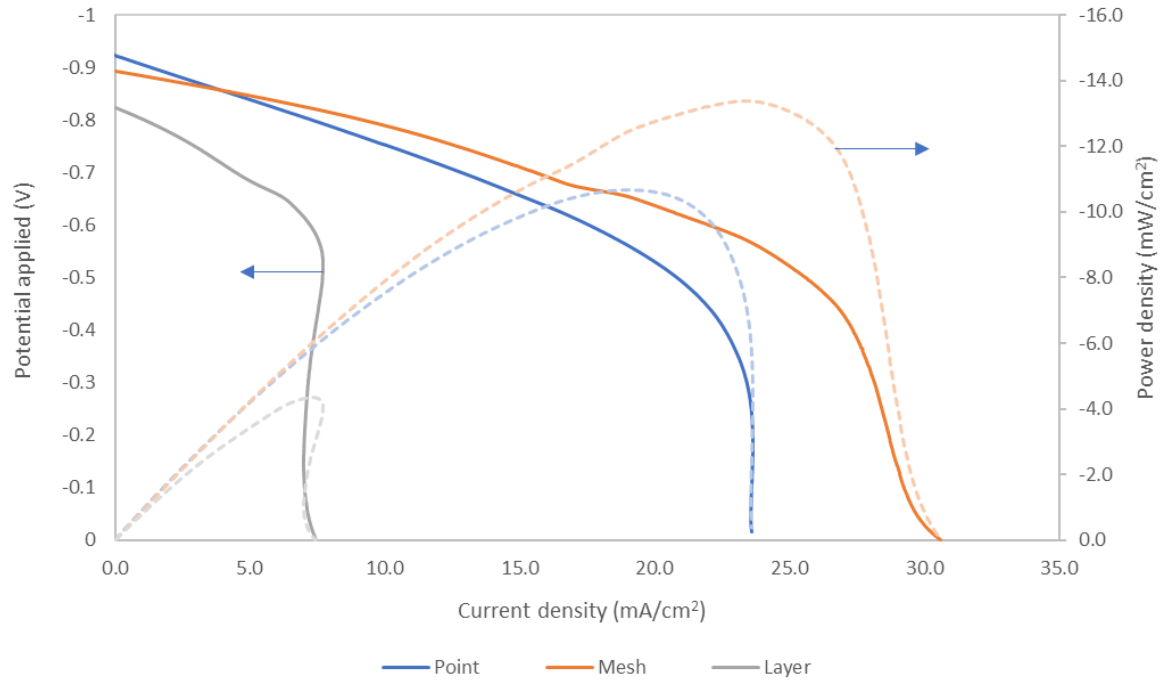


Figure 6.1: V-I curves of Point, Mesh and Layer current collector at 750 °C

As shown in Figure 6.1, the best cell performance was obtained from the cell with mesh type current collector, which has current density of 30.6 mA/cm<sup>2</sup> and power density of 13.4 mW/cm<sup>2</sup>. Following the mesh type current collector, it was the cell with point type current collector with current density of 24 mA/cm<sup>2</sup> and power density of 10.7 mW/cm<sup>2</sup>. Meanwhile, cell with layer type current collector has shown the worst performance with current density of 7.4 mA/cm<sup>2</sup> and power density of 4.3 mW/cm<sup>2</sup>. Table 6.1 summarizes the performance values of the cells.

Table 6.1: Performance of cells corresponding to Point, Mesh and Layer current collectors

	<b>I<sub>max</sub></b> <b>(mA/cm<sup>2</sup>)</b>	<b>P<sub>max</sub></b> <b>(mW/cm<sup>2</sup>)</b>
Point	24	10.7
Mesh	30.6	13.4
Layer	7.4	4.3

Cells were monitored via EIS measurements once LSV measurements have been completed and OCV values have stabilized to obtain further insight of the cell performances. Nyquist plots recorded employing different current collectors at 750 °C were shown in Figure 6.2. Equivalent circuits illustrated in Figure 4.5 fitted reasonably well with Nyquist plots obtained shown in Figure 6.2 with the goodness of fit or chi-squared ( $\chi^2$ ) values being  $10^{-3}$ .

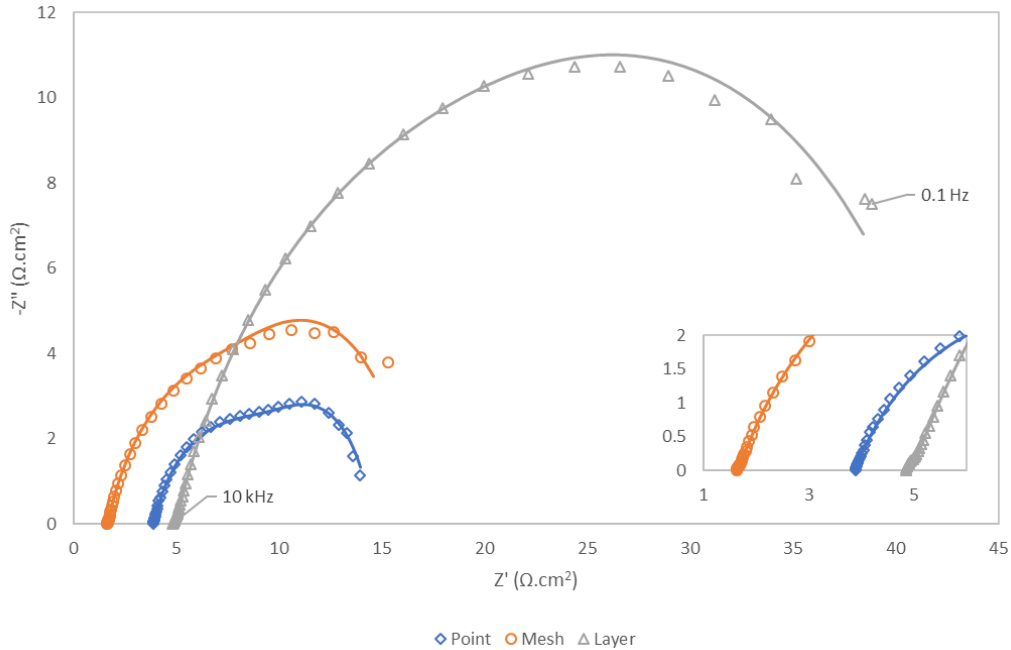


Figure 6.2: Nyquist plots of Point, Mesh and Layer current collector at 750 °C. The inset shows the close-up look of the Nyquist plots.

The values of resistive elements obtained from fitting Nyquist plot in Figure 6.2 were summarized in Table 6.2 and it shows that the cell resistance was significantly affected by the current collector configurations. Cell with mesh-like paste current collector has exhibited the lowest Rohmic and R1 when compared to other configurations of current collector although with a slightly higher R2 relatively to cell with point type current collector. The cell with point type current collector has produced Rohmic and R1 that were in between Mesh-like paste and Layer paste current collector.

Nevertheless, it has displayed the lowest R2 value when compared to other cells. Meanwhile, cell with layer type current collector has shown the highest Rohmic, R1 and R2 amongst other cells.

Table 6.2: Values of resistors by fitting equivalent circuit (Figure 4.5) into Nyquist plots (Figure 6.2)

	<b>R<sub>ohmic</sub></b>	<b>R1</b>	<b>R2</b>	<b>R<sub>total</sub></b>
Point	3.86	0.08	10.70	14.64
Mesh	1.62	0.04	14.61	16.27
Layer	4.83	0.13	38.24	43.20

Applying mesh-like paste current collector on both electrodes as shown in Figure 6.3 has enhanced the triple phase boundary of the cell where there will be more contact area between current collector, electrodes and pyrolyzed palm shell. The contact area of mesh-like paste current collector was estimated to be 0.29 cm<sup>2</sup> which was three times higher than the contact area of point paste current collector which was 0.08 cm<sup>2</sup>. Therefore, the contact resistance of mesh-like paste current collector has reduced drastically, which then reduces the R<sub>ohmic</sub> of mesh-like paste current collector since contact resistance was considered as part of the R<sub>ohmic</sub>.

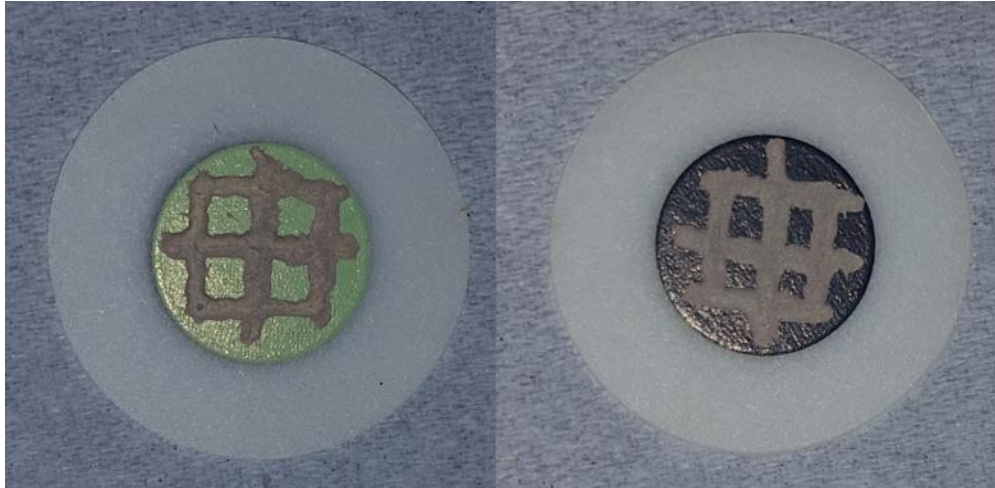


Figure 6.3: Mesh-like paste current collector applied to anode and cathode



The application of mesh-like paste current collector helps distribute the electrons evenly at the cathode as shown in Figure 6.4, unlike point type current collector where the electrons were concentrated at a point. Thus, the rate of oxygen reduction at cathode of mesh like paste current collector was high and the oxygen ions can reach a wider area of anode for carbon oxidation where the point type current collector was unable to achieve.

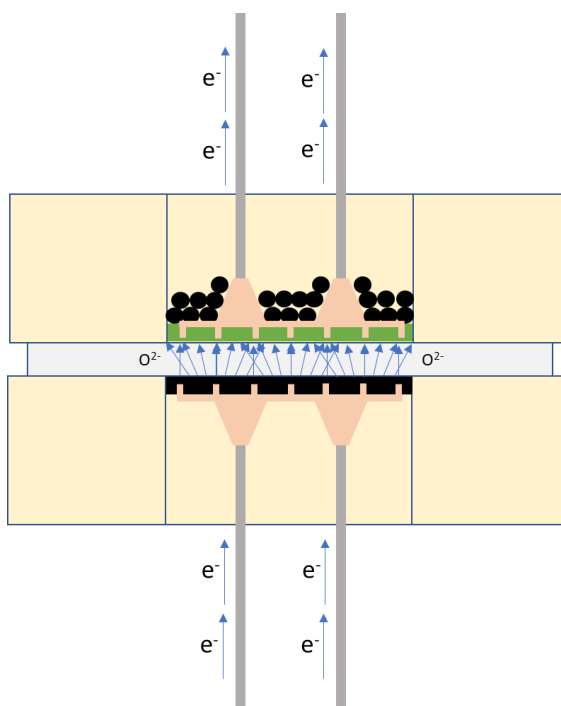


Figure 6.4: Schematic depicting the flow of electrons and oxygen ions in the mesh-like paste current collector

The high encounter rate between pyrolyzed palm shell and oxygen ions has resulted in higher rate of carbon oxidation and increased the production rate of CO and electrons. Besides that, the application of mesh-like paste current collector at anode helps shorten the traveling path of electrons flowing out of anode. As such, concentration polarization of mesh-like paste at high current loading was observed less prominent than the point type current collector because it was able to produce high amount of CO to sustain the demanding CO consumption during high current

loading. The shorten traveling path of electrons has contributed to low  $R_1$  that was observed for mesh-like paste current collector. Nonetheless, the mesh-like paste has had the surface of anode partially covered, hindering the diffusion process of CO into anode for further oxidation. Therefore, the  $R_2$  value of mesh-like paste current collector was slightly higher than Point type current collector. Despite having higher total resistance than Point type current collector, mesh-like paste current collector still produced highest current density and power density. The observation signals that direct carbon oxidation might play a dominant role than CO oxidation in determining the overall cell performance.

For the meantime, applying a layer of undiluted paste covering entire electrodes ( $0.79 \text{ cm}^2$ ) as shown in Figure 6.5 was detrimental to the overall cell performance in terms of current density, power density, and total resistance. The covered cathode has impeded the diffusion of  $\text{O}_2$  into the cathode for oxygen reduction while the covered anode has prevented palm shell from having direct contact with anode for carbon oxidation. Hence, the effective triple phase boundary of the cell has been halved. The undiluted layer paste also displayed the most prominent concentration polarization among the three types of current collector paste. This is due to the rate of carbon oxidation for undiluted layer type current collector was the lowest among the three configuration and CO was depleted faster than it can be supplied during high current loading. The sluggish rate of carbon oxidation was reflected in high magnitude of high-frequency arc and high  $R_1$  value also.

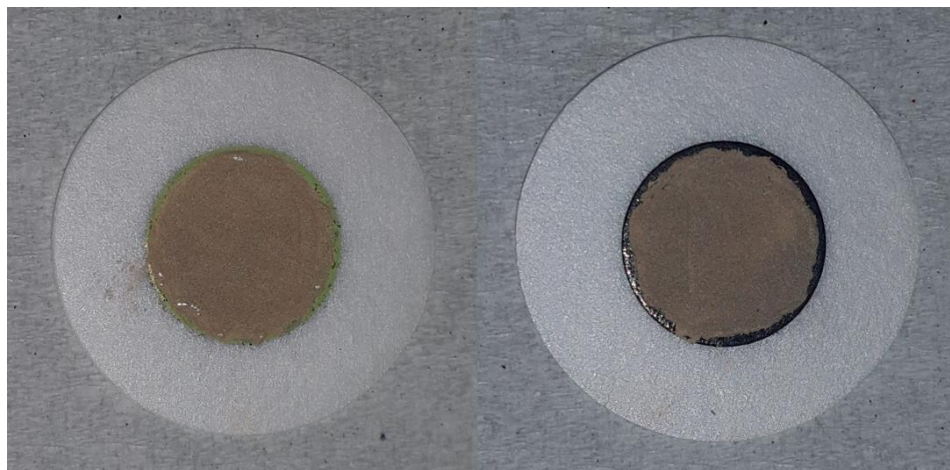


Figure 6.5: Layer paste current collector applied to anode and cathode

The high  $R_{ohmic}$  of layer type current collector suggests that the anode was mostly in NiO state as most of the CO generated from carbon oxidation could not reach anode to reduce it into Ni state. The high resistance of NiO has outweighed the lowered contact resistance brought by the enhanced contact points between current collector and anode. The large value of  $R_2$  of layer type current collector which reflected in the high magnitude of low-frequency arc in Figure 6.2 indicates that there was mass transfer limitation experienced by the cell which depends on the availability of CO near the interface between anode and electrolyte for further oxidation. The high  $R_{total}$  of layer type current collector has resulted in a poor current density and power density as observed in Figure 6.1.

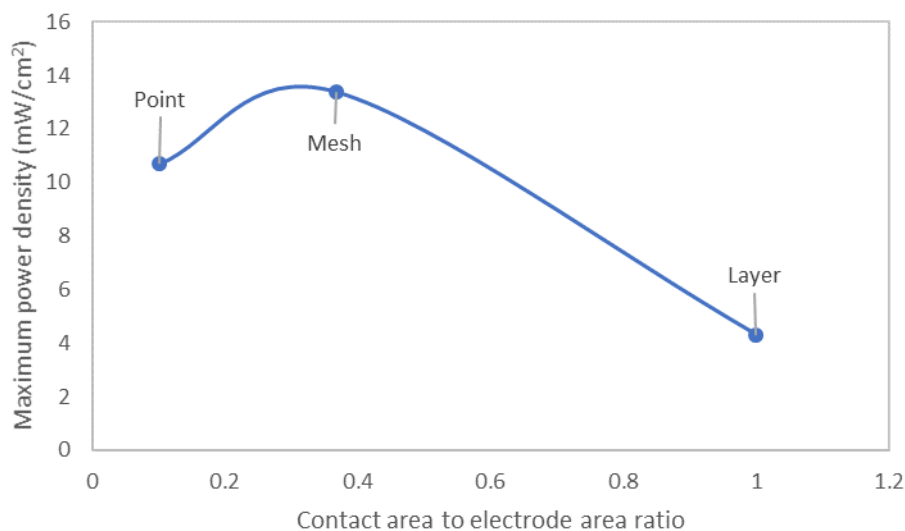


Figure 6.6: The maximum power density corresponding to contact area to electrode area ratio

Figure 6.6 illustrates the trend of maximum power density corresponding to different contact area to electrode area ratio. The maximum power density improved when the ratio increased from 0.1 to 0.36 ratio. Nonetheless, the value of the maximum power density dropped significantly when the contact area to electrode area ratio increased to 1. The observed trend signified that contact area between current collector and electrode, and the active area available for electrochemical reactions were important to the performance of DCFC. Similar results were obtained by Peiwen Li, et al. when the effect of geometries and distribution of current collectors on the power density in SOFC were studied through modeling approach [89]. The maximum power density of SOFC increased when the contact area of the current collector reduced from 1.5 mm to 0.6 mm. Peiwen Li, et al. correlated this observation to the increased of active area for electrochemical reactions. However, when the contact area of the current collector was further reduced lesser than 0.6 mm, the maximum power density dropped again and it was associated with the increased of ohmic resistance. The observed results have indicated that compromise between

contact area of current collector and the active area of electrodes for electrochemical reaction was essential to obtain optimum performance.

### 6.3 Conclusions

It is apparent that the availability of active area for electrochemical reactions and the contact area of current collector holds an important factor that will determine the DCFC performance. It is even more pronounced when tested with different configurations of current collector. The layer type current collector which has its electrodes covered entirely with Ag paste has the worst DCFC performance in all aspects while point type current collector which has the least electrodes covered by Ag paste has the second best DCFC performance. Mesh type current collector produced the best DCFC performance. Thus, it is important to have a balanced design that will not compromise the triple phase boundary to ensure optimum DCFC performance. All in all, cell that has  $0.79 \text{ cm}^2$  electrodes with 2Ag|2Ag current collector leads and mesh type current collector is able to yield the best DCFC performance.

## Chapter 7.

### Conclusion and Future works

#### 7.1 Conclusion

The effects of current collector on the performance of DCFC were successfully determined thorough LSV and EIS spectroscopy methods. The electrochemical performance of DCFC shows that the material and quantity of current collector leads and the configuration of current collector has significant impact on the performance of DCFC. By comparing the electrochemical performance of Ag|Ag, Pt|Ag, Ag|Pt and Pt|Pt, it was found that the electrochemical performance generated by Ag|Ag was better compared to Pt|Pt. As the experiment setup for both cells was identical, the differences of electrochemical performance were caused by the differences in electrical resistance inherited by the material itself. The low electrical resistance of Ag has facilitated the rate of electrons entering the cathode of DCFC and the rate of electrons leaving the anode of DCFC. This has enabled a higher rate of oxygen reduction at cathode and also the rate of carbon oxidation at anode. In the meantime, Pt has a high electrical resistance which dampened the rate of electrons entering and leaving DCFC. As such, the rate of oxygen reduction at cathode and rate of carbon oxidation at anode were low for Pt|Pt. The electrochemical performance of Pt|Ag and Ag|Pt were identical and they were in between Ag|Ag and Pt|Pt. Nevertheless, Pt|Ag has higher power density than Ag|Pt due to it has a higher voltage that was caused by the higher difference of electrons between cathode and anode. Observing the trend of electrochemical performance of the cells, cells with Ag at the cathode possessed higher power density indicated that the reaction at cathode played a prominent role in the overall electrochemical performance of a cell.

Other than that, by comparing the electrochemical performance of 2Ag|2Ag, 1Ag|2Ag, 2Ag|1Ag and 1Ag|1Ag, it could be observed that 2Ag|2Ag has significant higher electrochemical performance than 1Ag|1Ag while 1Ag|2Ag and 2Ag|1Ag have electrochemical performance that was in between 2Ag|2Ag and 1Ag|1Ag. This, in turn, suggested that installing additional current collector leads at electrodes has improved the contact area between current collector and electrodes and also enhanced the rate of electrons entering and leaving electrodes. Similarly, by observing the trend of electrochemical performance of the cells, cells with 2Ag at the cathode exhibited higher power density indicated that the reaction at cathode played a major role in the overall electrochemical performance of a cell.

Additionally, referring to the electrochemical performance of Point paste, Mesh-like paste and Layer paste current collector, it was found that cell with Mesh-like paste current collector has the optimum electrochemical performance, followed by Point paste current collector and Layer paste current collector. The electrochemical performance was observed to improve with the increase of the area of current collector due to the reduced contact resistance between current collector and electrodes. However, the said observation did not apply to layer paste current collector due to the anode was mostly blocked by Ag paste, and there was no direct contact between palm shell and anode which was vital for the carbon oxidation process. The observation suggested that direct carbon oxidation played a prominent role in the overall electrochemical performance of DCFC. Thus, it is important to have a balanced design that will not compromise either of the mechanisms to ensure optimum DCFC performance. By using LSV and EIS method, cell with  $0.79\text{cm}^2$  active area attached with two Ag current collector leads and mesh-like paste current collector at both sides of the electrodes yielded optimum DCFC performance.

## 7.2 Future works

Firstly, 30 mg of palm shell used in all the experiments is sufficient for 1 hour of electrochemical reactions only. The electrochemical reactions have caused small quantity of ashes to build upon the anode of DCFC. Since the quantity of ashes built up is small, it does not have significant impact on the results. However, for a long-term analysis, the quantity of ashes built upon the anode will be increased and above may affect the results of the analysis. As a result, to facilitate a long-term performance analysis, self-cleaning and self-feeding design is required to continuously purge out the built-up ashes and supply the carbon fuel directly to the fuel cell. There are a few designs that can be referred to, with the notable one being the tilted molten carbonate DCFC design by Cooper et al [14]. The tilted DCFC will cause the ashes to be pulled down by gravity and ensuring constant contact between the palm shell and anode.

Secondly, DCFC with thick layer of electrolyte and Ag current collector at an operating temperature of 750 °C has shown to produce the highest electrochemical performance amongst the other material of current collector. Nevertheless, operating temperature of 750 °C is rather high to be widely adopted due to significant disadvantages associated with high cost of materials and long startup time. On the other hand, reducing the operating temperature of current DCFC setup to less than 700 °C may pose a rather high  $R_{ohmic}$  to the system due to the reduced conductivity of ions caused by the thick layer of YSZ electrolyte. Hence, for a lower temperature of less than 700 °C, it is recommended that anode supported cell which has thin layer of electrolyte should be employed in future experiments as the  $R_{ohmic}$  of the cell is not impacted due to the shorter travel distance of oxygen ions.

Lastly, the degradation of Ag current collector lead was severed under a high temperature for long hours as observed by Meulenberg et al.[34]. However, the degradation of Ag can be



minimized by reducing the area of Ag expose to air with a protective coating. Various deposition techniques such as electroplating, sputtering, dip coating, spic coating, screen printing, tape casting or plasma spraying can be an option to apply the protective coating. As a result, it is advisable that a controllable, reproducible and cost-effective coating process is employed if any of the researchers wish to consider the above suggestion as their research topic.

## Chapter 8.

### References

1. Berhad, T.N., *TNB Annual Reports*. 2014.
2. Giddey, S., et al., *A comprehensive review of direct carbon fuel cell technology*. Progress in Energy and Combustion Science, 2012. **38**(3): p. 360-399.
3. Stolten, D. and B. Emonts, *Fuel Cell Science and Engineering: Materials, Processes, Systems and Technology*. Fuel Cell Science and Engineering: Materials, Processes, Systems and Technology. Vol. 1-2. 2012: Wiley-VCH.
4. Basu, S., *Recent trends in fuel cell science and technology*. Recent Trends in Fuel Cell Science and Technology. 2007: Springer New York. 1-375.
5. Grove, W.R., *LVI. On a new voltaic combination*. Philosophical Magazine Series 3, 1838. **13**(84): p. 430-431.
6. Deleebeeck, L. and K.K. Hansen, *Hybrid direct carbon fuel cells and their reaction mechanisms—a review*. Journal of Solid State Electrochemistry, 2014. **18**(4): p. 861-882.
7. Rady, A.C., et al., *Degradation Mechanism in a Direct Carbon Fuel Cell Operated with Demineralised Brown Coal*. Electrochimica Acta, 2014. **143**(0): p. 278-290.
8. Kulkarni, A., S. Giddey, and S.P.S. Badwal, *Yttria-doped ceria anode for carbon-fueled solid oxide fuel cell*. Journal of Solid State Electrochemistry, 2015. **19**(2): p. 325-335.
9. Cao, D., Y. Sun, and G. Wang, *Direct carbon fuel cell: Fundamentals and recent developments*. Journal of Power Sources, 2007. **167**(2): p. 250-257.
10. Zecevic, S., E.M. Patton, and P. Parhami, *Carbon-air fuel cell without a reforming process*. Carbon, 2004. **42**(10): p. 1983-1993.
11. Rady, A.C., et al., *Review of Fuels for Direct Carbon Fuel Cells*. Energy & Fuels, 2012. **26**(3): p. 1471-1488.
12. Elleuch, A., et al., *2-D numerical modeling and experimental investigation of electrochemical mechanisms coupled with heat and mass transfer in a planar direct carbon fuel cell*. Journal of Power Sources, 2014. **248**: p. 44-57.
13. Elleuch, A., et al., *Experimental investigation of direct carbon fuel cell fueled by almond shell biochar: Part I. Physico-chemical characterization of the biochar fuel and cell performance examination*. International Journal of Hydrogen Energy, 2013. **38**(36): p. 16590-16604.
14. Cooper, J.F. *Direct conversion of coal and coal-derived carbon in fuel cells*. in *Second International Conference on Fuel Cell Science, Engineering and Technology*. 2004. Rochester, NY.
15. Nease, J. and T.A. Adams II, *Comparative life cycle analyses of bulk-scale coal-fueled solid oxide fuel cell power plants*. Applied Energy, 2015. **150**: p. 161-175.
16. Kaklidis, N., et al., *Effect of carbon type on the performance of a direct or hybrid carbon solid oxide fuel cell*. RSC Advances, 2014. **4**(36): p. 18792-18800.
17. Elleuch, A., K. Halouani, and Y. Li, *Investigation of chemical and electrochemical reactions mechanisms in a direct carbon fuel cell using olive wood charcoal as sustainable fuel*. Journal of Power Sources, 2015. **281**: p. 350-361.
18. Konsolakis, M., et al., *Assessment of biochar as feedstock in a direct carbon solid oxide fuel cell*. RSC Advances, 2015. **5**(90): p. 73399-73409.
19. Munnings, C., et al., *Biomass to power conversion in a direct carbon fuel cell*. International Journal of Hydrogen Energy, 2014. **39**(23): p. 12377-12385.
20. Desclaux, P., et al., *Actual State of Technology in Direct Carbon Fuel Cells*, in *Zeitschrift für Physikalische Chemie International journal of research in physical chemistry and chemical physics*. 2013. p. 627.

21. Zecevic, S., E.M. Patton, and P. Parhami, *Direct electrochemical power generation from carbon in fuel cells with molten hydroxide electrolyte*. Chemical Engineering Communications, 2005. **192**(10-12): p. 1655-1670.
22. Huijsmans, J.P.P., et al., *Analysis of endurance issues for MCFC*. 6th Grove Fuel Cell Symposium : Fuel Cells - The Competitive Option for Sustainable Energy Supply, 2000. **86**(1): p. 117-121.
23. Pointon, K., et al., *The development of a carbon-air semi fuel cell*. Journal of Power Sources, 2006. **162**(2 SPEC. ISS.): p. 750-756.
24. Li, C., Y. Shi, and N. Cai, *Effect of contact type between anode and carbonaceous fuels on direct carbon fuel cell reaction characteristics*. Journal of Power Sources, 2011. **196**(10): p. 4588-4593.
25. Chen, X.J., K.A. Khor, and S.H. Chan, *Identification of O<sub>2</sub> reduction processes at yttria stabilized zirconia/doped lanthanum manganite interface*. Journal of Power Sources, 2003. **123**(1): p. 17-25.
26. Dudek, M. and P. Tomczyk, *Composite fuel for direct carbon fuel cell*. Catalysis Today, 2011. **176**(1): p. 388-392.
27. Escudero, M.J., et al., *A kinetic study of oxygen reduction reaction on La<sub>2</sub>NiO<sub>4</sub> cathodes by means of impedance spectroscopy*. Journal of Electroanalytical Chemistry, 2007. **611**(1-2): p. 107-116.
28. Kulkarni, A., S. Giddey, and S.P.S. Badwal, *Electrochemical performance of ceria-gadolinia electrolyte based direct carbon fuel cells*. Solid State Ionics, 2011. **194**(1): p. 46-52.
29. Lee, I., et al., *Ash-free coal as fuel for direct carbon fuel cell*. Science China Chemistry, 2014. **57**(7): p. 1010-1018.
30. Lee, Y.-K., et al., *Conditioning effects on La<sub>1-x</sub>Sr<sub>x</sub>MnO<sub>3</sub>-yttria stabilized zirconia electrodes for thin-film solid oxide fuel cells*. Journal of Power Sources, 2003. **115**(2): p. 219-228.
31. Nguyen, T.L., et al., *Fabrication and Characterization of Anode-Supported Tubular SOFCs with Zirconia-Based Electrolyte for Reduced Temperature Operation*. Journal of The Electrochemical Society, 2004. **151**(8): p. A1230-A1235.
32. Rady, A.C., et al., *Direct carbon fuel cell operation on brown coal*. Applied Energy, 2014. **120**(0): p. 56-64.
33. Jiao, Z. and N. Shikazono, *Study on the influence of current collector on the sudden deterioration of solid oxide fuel cell anode performance*. Journal of Fuel Cell Science and Technology, 2014. **11**(2).
34. Meulenbergh, W.A., et al., *Improved contacting by the use of silver in solid oxide fuel cells up to an operating temperature of 800 °C*. Journal of Materials Science, 2001. **36**(13): p. 3189-3195.
35. Guo, Y., et al., *Significant impact of the current collection material and method on the performance of Ba<sub>0.5</sub>Sr<sub>0.5</sub>Co<sub>0.8</sub>Fe<sub>0.2</sub>O<sub>3-δ</sub> electrodes in solid oxide fuel cells*. Journal of Power Sources, 2011. **196**(13): p. 5511-5519.
36. Jiang, C. and J.T.S. Irvine, *Catalysis and oxidation of carbon in a hybrid direct carbon fuel cell*. Journal of Power Sources, 2011. **196**(17): p. 7318-7322.
37. Chen, Y., et al., *Role of silver current collector on the operational stability of selected cobalt-containing oxide electrodes for oxygen reduction reaction*. Journal of Power Sources, 2012. **210**: p. 146-153.
38. Jain, S.L., et al., *Electrochemical performance of a hybrid direct carbon fuel cell powered by pyrolysed MDF*. Energy & Environmental Science, 2009. **2**(6): p. 687-693.
39. Deleebeeck, L., et al., *Direct Coal Oxidation in Modified Solid Oxide Fuel Cells*. ECS Transactions, 2015. **68**(1): p. 2685-2694.
40. Desclaux, P., et al., *Influence of the carbon/anode interaction on direct carbon conversion in a SOFC*. International Journal of Electrochemical Science, 2013. **8**(7): p. 9125-9132.
41. Kouchachvili, L. and M. Ikura, *Performance of direct carbon fuel cell*. International Journal of Hydrogen Energy, 2011. **36**(16): p. 10263-10268.
42. Guillodo, M., P. Vernoux, and J. Fouletier, *Electrochemical properties of Ni-YSZ cermet in solid oxide fuel cells. Effect of current collecting*. Solid State Ionics, 2000. **127**(1-2): p. 99-107.

43. Fu, X.-Z., et al., *Surface modified Ni foam as current collector for syngas solid oxide fuel cells with perovskite anode catalyst*. International Journal of Hydrogen Energy, 2010. **35**(20): p. 11180-11187.
44. Antunes, R. and M. Skrzypkiewicz, *Chronoamperometric investigations of electro-oxidation of lignite in direct carbon bed solid oxide fuel cell*. International Journal of Hydrogen Energy, 2015. **40**(12): p. 4357-4369.
45. De Silva, K.C.R., B.J. Kaseman, and D.J. Bayless, *Silver (Ag) as anode and cathode current collectors in high temperature planar solid oxide fuel cells*. International Journal of Hydrogen Energy, 2011. **36**(1): p. 779-786.
46. Jiang, S.P., J.G. Love, and L. Apateanu, *Effect of contact between electrode and current collector on the performance of solid oxide fuel cells*. Solid State Ionics, 2003. **160**(1-2): p. 15-26.
47. Kendall, K. and M. Kendall, *High-Temperature Solid Oxide Fuel Cells for the 21st Century: Fundamentals, Design and Applications: Second Edition*. High-Temperature Solid Oxide Fuel Cells for the 21st Century: Fundamentals, Design and Applications: Second Edition. 2015: Elsevier Inc. 1-508.
48. Huang, H., et al., *High-Performance Ultrathin Solid Oxide Fuel Cells for Low-Temperature Operation*. Journal of The Electrochemical Society, 2007. **154**(1): p. B20-B24.
49. Bloomberg, *Commodities: Platinum (XPTUSD:CUR)*. 2015.
50. Simner, S.P., et al., *Performance of a novel La(Sr)Fe(Co)O<sub>3</sub>-Ag SOFC cathode*. Journal of Power Sources, 2006. **161**(1): p. 115-122.
51. Wilkinson, L.T. and J.H. Zhu, *Ag-Perovskite Composite Materials for SOFC Cathode-Interconnect Contact*. Journal of The Electrochemical Society, 2009. **156**(8): p. B905-B912.
52. Yang, Z., et al., *Electrical contacts between cathodes and metallic interconnects in solid oxide fuel cells*. Journal of Power Sources, 2006. **155**(2): p. 246-252.
53. Bloomberg, *Commodities: Silver (SI1:COM)*. 2015.
54. Kim, J.-H., et al., *Degradation of cathode current-collecting materials for anode-supported flat-tube solid oxide fuel cell*. Journal of Power Sources, 2009. **188**(2): p. 447-452.
55. Damiano Bonaccorso, A., et al., *Studies of current collection configurations and sealing for tubular hybrid-DCFC*. International Journal of Hydrogen Energy.
56. Deleebeeck, L. and K.K. Hansen, *Hybrid Direct Carbon Fuel Cell Performance With Anode Current Collector Material*. Journal of Fuel Cell Science and Technology, 2016. **12**(6): p. 064501-064501.
57. Gong, Y., C. Qin, and K. Huang, *Can Silver Be a Reliable Current Collector for Electrochemical Tests?* ECS Electrochemistry Letters, 2013. **2**(1): p. F4-F7.
58. Hatchwell, C.E., N.M. Sammes, and K. Kendall, *Cathode current-collectors for a novel tubular SOFC design*. Journal of Power Sources, 1998. **70**(1): p. 85-90.
59. Lowe, R.M., *The evaporation of silver in oxygen, nitrogen and vacuum*. Acta Metallurgica, 1964. **12**(10): p. 1111-1118.
60. Hondros, E.D. and A.J.W. Moore, *Evaporation and thermal etching*. Acta Metallurgica, 1960. **8**(9): p. 647-653.
61. Janek, J. and G. Korte, *Matter transport in temperature gradients — the heat of transport of silver in  $\beta$ -Ag<sub>2</sub> +  $\delta$ S*. Solid State Ionics, 1996. **85**(1-4): p. 305-311.
62. Ho, P.S. and H.B. Huntington, *Electromigration and void observation in silver*. Journal of Physics and Chemistry of Solids, 1966. **27**(8): p. 1319-1329.
63. Simner, S.P., et al., *Performance Variability of La ( Sr ) FeO<sub>3</sub> SOFC Cathode with Pt, Ag, and Au Current Collectors*. Journal of The Electrochemical Society, 2005. **152**(9): p. A1851-A1859.
64. Zheludkevich, M.L., et al., *Oxidation of silver by atomic oxygen*. Oxidation of Metals, 2004. **61**(1-2): p. 39-48.
65. Biemann, M., et al., *AgO investigated by photoelectron spectroscopy: Evidence for mixed valence*. Physical Review B - Condensed Matter and Materials Physics, 2002. **65**(23): p. 2354311-2354315.

66. Atwater, J.E., *Complex dielectric permittivities of the Ag<sub>2</sub>O-Ag<sub>2</sub>CO<sub>3</sub> system at microwave frequencies and temperatures between 22 °C and 189 °C*. Applied Physics A: Materials Science and Processing, 2002. **75**(5): p. 555-558.
67. Wan, Y., et al., *Corrosion behavior of copper at elevated temperature*. International Journal of Electrochemical Science, 2012. **7**(9): p. 7902-7914.
68. Zhu, Y., K. Mimura, and M. Isshiki, *Oxidation mechanism of copper at 623-1073 K*. Materials Transactions, 2002. **43**(9): p. 2173-2176.
69. Valerii, V.B. and A.A. Klimashin, *High-temperature oxidation of copper*. Russian Chemical Reviews, 2013. **82**(3): p. 273.
70. Park, J.H. and K. Natesan, *Oxidation of copper and electronic transport in copper oxides*. Oxidation of Metals, 1993. **39**(5-6): p. 411-435.
71. De Los Santos Valladares, L., et al., *Crystallization and electrical resistivity of Cu<sub>2</sub>O and CuO obtained by thermal oxidation of Cu thin films on SiO<sub>2</sub>/Si substrates*. Thin Solid Films, 2012. **520**(20): p. 6368-6374.
72. Rolle, A., et al., *Evidence of the Current Collector Effect: Study of the SOFC Cathode Material Ca<sub>3</sub>Co<sub>4</sub>O<sub>9+δ</sub>*. Fuel Cells, 2012. **12**(2): p. 288-301.
73. Boukamp, B.A., et al., *Impedance of thin film cathodes: Thickness and current collector dependence*. Solid State Ionics, 2015. **283**: p. 81-90.
74. Bi, Z.H. and J.H. Zhu, *Effect of Current Collecting Materials on the Performance of the Double-Perovskite Sr<sub>2</sub>MgMoO<sub>6-δ</sub> Anode*. Journal of The Electrochemical Society, 2011. **158**(6): p. B605-B613.
75. Wang, G., et al., *Factors of cathode current-collecting layer affecting cell performance inside solid oxide fuel cell stacks*. International Journal of Hydrogen Energy, 2014. **39**(31): p. 17836-17844.
76. Wu, W., et al., *Effect of contact method between interconnects and electrodes on area specific resistance in planar solid oxide fuel cells*. Fuel Cells, 2013. **13**(5): p. 743-750.
77. Giddey, S., et al., *Performance evaluation of a tubular direct carbon fuel cell operating in a packed bed of carbon*. Energy, 2014. **68**(0): p. 538-547.
78. Cherepy, N.J., et al., *Direct Conversion of Carbon Fuels in a Molten Carbonate Fuel Cell*. Journal of The Electrochemical Society, 2005. **152**(1): p. A80-A87.
79. Chien, A.C., et al., *Performance of Direct Carbon Fuel Cells Operated on Coal and Effect of Operation Mode*. Journal of The Electrochemical Society, 2014. **161**(5): p. F588-F593.
80. Giddey, S., et al., *Composite anodes for improved performance of a direct carbon fuel cell*. Journal of Power Sources, 2015. **284**(0): p. 122-129.
81. Canavar, M. and Y. Kaplan, *Effects of mesh and interconnector design on solid oxide fuel cell performance*. International Journal of Hydrogen Energy, (0).
82. Sasaki, K., et al., *Microstructure-Property Relations of Solid Oxide Fuel Cell Cathodes and Current Collectors: Cathodic Polarization and Ohmic Resistance*. Journal of The Electrochemical Society, 1996. **143**(2): p. 530-543.
83. Lim, S.H., *Utilization of biomass as fuel source for direct carbon fuel cell*.
84. Li, C., Y. Shi, and N. Cai, *Performance improvement of direct carbon fuel cell by introducing catalytic gasification process*. Journal of Power Sources, 2010. **195**(15): p. 4660-4666.
85. Matula, R.A., *Electrical resistivity of copper, gold, palladium, and silver*. Journal of Physical and Chemical Reference Data, 1979. **8**(4): p. 1147-1298.
86. Chien, A.C. and J.T.S. Irvine, *19 - Hybrid Molten Carbonate/Solid Oxide Direct Carbon Fuel Cells*, in *Molten Salts Chemistry*, F.L. Groult, Editor. 2013, Elsevier: Oxford. p. 403-414.
87. C.W.C., *Thermophysical Data on Platinum: Resistivity and Conductivity Values Recommended*. Platinum Metals Review, 1984. **28**(4): p. 169.
88. Malzbender, J., E. Wessel, and R.W. Steinbrech, *Reduction and re-oxidation of anodes for solid oxide fuel cells*. Solid State Ionics, 2005. **176**(29-30): p. 2201-2203.

89. Li, P., G. Tao, and H. Liu, *Effect of the geometries of current collectors on the power density in a solid oxide fuel cell*. International Journal of Energy and Environmental Engineering, 2011. **2**(3): p. 1-11.